CHAPTER

# 3

# Statics

## 3.1 INTRODUCTION

Static and kinetostatic relations play basic role in kinetostatic analysis, optimization, and control. This chapter is divided in eight sections. In the following section, force/moment relations are derived from the principle of virtual work and notations for wrenches and spatial forces are introduced. In Section 3.3, contact joint models with frictional constraints are discussed. Section 3.4 focuses on kinetostatic relations in independent closed-loop chains. Section 3.5 tackles the important problem of body wrench distribution at the contact joints. The kinetostatic relations of a humanoid robot comprising both independent and interdependent closed chains are explained in Section 3.6. Section 3.7 analyzes the stability of a static posture and discusses statics-based optimization. The duality relations of the static and kinematic relations pertinent to a humanoid robot are explained in Section 3.8.

## 3.2 WRENCH AND SPATIAL FORCE

Let $\boldsymbol{f} \in \Re^3$ denote the force vector and $\boldsymbol{m}_P \in \Re^3$ be the moment vector acting at point $P$ on a robot link. The two vectors are stacked to form a 6D vector that represents a *wrench*. We have

$$\mathcal{F}_P = \begin{bmatrix} \boldsymbol{f}^T & \boldsymbol{m}_P^T \end{bmatrix}^T \in \Re^6.$$

Similarly to the term "twist," the term "wrench" originates from the theory of screws [4]. The two components of a wrench are referred to as bivectors, as it was the case with a twist. The term has also been adopted in the robotics field [49,19]. A wrench is an element of $se^*(3)$, the dual space of $se(3)$. Wrenches and twists form a duality relation, whereby their dot product determines the instantaneous power: $\mathcal{V} \cdot \mathcal{F}$. This quantity can be expressed in coordinate form as $\mathcal{V}_P^T \mathcal{F}_P = \boldsymbol{v}_P^T \boldsymbol{f} + \boldsymbol{\omega}^T \boldsymbol{m}_P$. Similarly to twists, wrenches can be represented either in the inertial or the body frame. In the former case, the term *spatial force* is used [24]. Spatial force can be considered as an operator that, given an arbitrary point $P$ on the rigid body, produces the total moment about that point, i.e.

$$\boldsymbol{m}_O = -[\boldsymbol{r}^{\times}_{\overleftarrow{OP}}]\boldsymbol{f} + \boldsymbol{m}_P, \tag{3.1}$$

where $\boldsymbol{r}_{\overleftarrow{OP}} = \boldsymbol{r}_O - \boldsymbol{r}_P$.

Furthermore, it is straightforward to show ([49], p. 62) that a wrench, acting at point $P$ in a given coordinate frame, can be transformed into an equivalent wrench, acting at point $O$ in a different frame, via the transposed spatial transform for twists. Consider, for example, two wrenches ${}^{W}\mathcal{F}_O$ and ${}^{B}\mathcal{F}_P$. These wrenches will be equivalent if the following instantaneous power relation holds:

$$({}^{W}\mathcal{V}_O)^T({}^{W}\mathcal{F}_O) = ({}^{B}\mathcal{V}_P)^T({}^{B}\mathcal{F}_P).$$

Since ${}^{W}\mathcal{V}_O^T = ({}^{B}\mathcal{V}_P)^T({}^{W}\mathbb{X}_{B_{\overleftarrow{OP}}})^T$ (cf. (2.6)), it follows that

$${}^{B}\mathcal{F}_O = {}^{W}\mathbb{X}_{B_{\overleftarrow{OP}}}^{-T}({}^{W}\mathcal{F}_P) = {}^{B}\mathbb{X}_{W_{\overleftarrow{OP}}}^{T}({}^{W}\mathcal{F}_P), \tag{3.2}$$

for any ${}^{W}\mathcal{V}_O$. Using (2.6), the transpose can be expressed as

$$\begin{aligned} {}^{B}\mathbb{X}_{W_{\overleftarrow{OP}}}^{T} &= {}^{B}\mathbb{T}_{\overleftarrow{OP}}^{T}\,{}^{W}\mathbb{R}_B^T \\ &= \begin{bmatrix} \boldsymbol{E} & \boldsymbol{0} \\ -[{}^{B}\boldsymbol{r}_{\overleftarrow{OP}}^{\times}]^T & \boldsymbol{E} \end{bmatrix} \begin{bmatrix} {}^{W}\boldsymbol{R}_B^T & \boldsymbol{0} \\ \boldsymbol{0} & {}^{W}\boldsymbol{R}_B^T \end{bmatrix}. \end{aligned} \tag{3.3}$$

Quite often, spatial forces are subjected to pure translations. From the above relations one obtains

$$\begin{aligned} \mathcal{F}_O &= \mathbb{T}_{\overleftarrow{OP}}^{T}\mathcal{F}_P \\ &= \begin{bmatrix} \boldsymbol{E} & \boldsymbol{0} \\ -[\boldsymbol{r}_{\overleftarrow{OP}}^{\times}] & \boldsymbol{E} \end{bmatrix} \mathcal{F}_P. \end{aligned} \tag{3.4}$$

Note that, in this transformation rule for wrenches, the overarrow notation in the subscript points in the correct direction. It is straightforward to confirm that the moment component of the resultant wrench is in agreement with (3.1).

The wrench representation leads to compact notations but should be used with care because of the nonuniform dimensions of the bivectors [22,21].

## 3.3 CONTACT JOINTS: STATIC RELATIONS

Two types of contact joints, with and without friction, were introduced in Section 2.9.1 and examined from the viewpoint of kinematics. It was clarified that only frictionless contact joints enable pure relative motion. In what follows, contact joints will be examined from the viewpoint of statics. Both, contact joints with and without friction, are relevant from this point of view. Indeed, these two types of joints can transmit force/moment components along the constrained motion directions.

### 3.3.1 Static Models of Frictionless Contact Joints

Denote by $\overline{\mathcal{F}}_k \in \Re^{c_k}$ ($k \in \{e_r, e_l\}$, $e \in \{H, F\}$) the force/moment components that can be transmitted along the constrained motion directions at a frictionless contact joint. These components determine the contact joint wrench, i.e.

$$\mathcal{F}_k = {}^k\mathbb{B}_c \overline{\mathcal{F}}_k. \tag{3.5}$$

Here ${}^k\mathbb{B}_c \in \Re^{6\times c_k}$ is the motion constraint (wrench) subspace basis at contact joint $k$. Recall that this basis is complementary to the velocity transform basis ${}^k\mathbb{B}_m \in \Re^{6\times\eta_k}$ defined in Section 2.9.3.

Further on, a contact joint may impose *bilateral* and/or *unilateral* motion constraints. For example, when an object with handles is firmly grasped by the hands, bilateral constraints will be imposed. Such contact constraints can also be imposed with a loose grasp. Recall the example depicted in Fig. 2.11; the frictionless cylindrical contact joints at the hands can transmit four force/moment components: two forces in the cross-sectional plane of the rod and two out-of-plane moments. The transmission of these forces and moments is bidirectional; hence, the motion constraints at these two hand contacts are characterized as frictionless and bilateral. Thus:

$${}^{H_j}\mathbb{B}_c = \begin{bmatrix} 1 & 0 & 0 & 0 \\ 0 & 0 & 0 & 0 \\ 0 & 1 & 0 & 0 \\ 0 & 0 & 1 & 0 \\ 0 & 0 & 0 & 0 \\ 0 & 0 & 0 & 1 \end{bmatrix}, \quad \overline{\mathcal{F}}_{H_j} = \begin{bmatrix} f_x \\ f_z \\ m_x \\ m_z \end{bmatrix}. \tag{3.6}$$

Since all constraints are bilateral, no inequalities appear for the magnitudes.

Next, consider the contact joints at the feet in a double stance. These contact joints impose unilateral constraints in the vertical direction: the feet can only push on the ground, they cannot pull it. Contact joints with unilateral constraints are met in fact quite often; besides the feet contacts, such joints also appear in multifinger grasping [49], when bodies impact, and so on. Unilateral constraints involve inequalities and are therefore more difficult to model than the bilateral ones [46]. When the contact joints at the feet are frictionless, they can transmit three force/moment components: one vertical force parallel to the ground normal and two tangential (out-of-plane) moments. The vertical force, however, can be transmitted only downward. Thus,

$${}^{F_j}\mathbb{B}_c = \begin{bmatrix} 0 & 0 & 0 \\ 0 & 0 & 0 \\ 1 & 0 & 0 \\ 0 & 1 & 0 \\ 0 & 0 & 1 \\ 0 & 0 & 0 \end{bmatrix}, \quad \overline{\mathcal{F}}_{F_j} = \begin{bmatrix} f_z \\ m_x \\ m_y \end{bmatrix}. \tag{3.7}$$

Here $f_z \geq 0$ is the normal force magnitude resulting from the unilateral constraint; $\pm m_x$, $\pm m_y$ are tangent moment magnitudes stemming from bilateral constraints. As already mentioned,

a positive *reaction* normal force indicates a compressive force at a unilateral contact, by convention.

Further on, note that unilateral constraints are characterized by the following kinematic conditions:

$$v_z = 0$$

and

$$\dot{v}_z \geq 0,$$

$v_z$ standing for the relative speed between the contacting surfaces. This speed is related to the contact state (initial contact condition) and is common for any type of contact joint. The relative acceleration $\dot{v}_z$, on the other hand, is related to the future state and is specific for unilateral contacts. Under this condition, the bodies cannot interpenetrate; it signifies that the contact will be maintained with zero normal acceleration. The main contact condition is expressed via the *complementarity condition* [61],

$$f_z \dot{v}_z = 0. \tag{3.8}$$

Accordingly, since the unilateral contact is characterized by a repulsive normal contact force (by assumption), it can only be maintained with zero normal acceleration [63]. Complementarity then implies that if $\dot{v}_z$ ceases to be zero, the contact is going to brake and, hence, the normal force must become zero ($f_z = 0$) [5].

### 3.3.2 Models of Contact Joints With Friction

Frictionless contact joint models are used to represent idealized contact conditions. In real life, motion along the "unconstrained" directions is always obstructed by force/moment components stemming from friction. Friction plays an important role in locomotion and dexterous object manipulation with the fingers and hands. Thus, it is important to construct appropriate models for contact joints with friction. Such models will be introduced in what follows.

A contact joint with friction that does not slide can be characterized as a fully constrained joint, i.e. $c_k = 6$, $\eta_k = 0$. Recall that a "welded"-type joint was characterized in the same way in Section 2.9.1. The welded joint does not transmit any motion, whatever the applied external wrench. In the case of a contact joint with friction, on the other hand, motion (sliding or slipping) may occur in the directions of action of friction forces or moments (the tangential directions). These directions will be henceforth referred to as the directions of *soft constraints*. They need to be distinguished from those that do not admit motion, irrespective of the magnitude of the applied friction wrench (i.e. the normal directions). The latter will be referred to as the directions of *hard constraints*. The hard- and soft-constraint directions are determined by the basis vectors ${}^k\mathbb{B}_c \in \Re^{6\times c_k^h}$ and ${}^k\mathbb{B}_m \in \Re^{6\times c_k^s}$, respectively, where $c_k = c_k^h + c_k^s$.

#### *Point-Contact Model*

Consider first a point-contact joint model. Without friction, the only force component transmitted across the joint is the force $f_{k_z}$ in the normal direction. This is the hard-constraint

direction. With friction, the forces $f_{k_x}$ and $f_{k_y}$ in the tangential directions will be transmitted as well. These are the soft-constraint directions. Point-contact joints are frequently used in multifinger grasping models. They are also quite useful to approximate the flat-surface contacts at the feet (planar contacts), as will be clarified shortly. Motion/force analysis and control at point-contact joints is based on the following *Coulomb friction model* [49]:

$$\sqrt{f_{k_x}^2 + f_{k_y}^2} > \mu_k f_{k_z},$$

where $\mu_k > 0$ denotes the constant static friction coefficient. Hence, the tangential forces that can be used by the robot at the contact must lie within the set

$$\left\{ FC_k : \sqrt{f_{k_x}^2 + f_{k_y}^2} \leq \mu_k f_{k_z},\ f_{k_z} \geq 0 \right\}. \tag{3.9}$$

This set is represented geometrically via the *friction cone*, constructed by rotating a line inclined by the angle $\tan^{-1} \mu_k$ w.r.t. the normal and passing through the contact point. Note that since $f_{k_z}$ is nonnegative (i.e. it is a *reaction* force), only the half-cone in the positive direction is relevant.

When the above friction cone condition cannot be satisfied, the contact joint begins to slide and the friction model changes from a static to a dynamic one. Under dynamic friction, the instantaneous power at the contact obeys the following relation [63]:

$$\mu_k f_{k_z} v_{k_t} + f_{k_t} \sqrt{v_{k_x}^2 + v_{k_y}^2} = 0,\ \ t \in \{x, y\}. \tag{3.10}$$

This means that while the contact joint slides, the contact force stays at the boundary of the friction cone, its direction being thereby opposite to the direction of the velocity of sliding.

When modeling contact joints at the fingertips, contacts with rolling are more realistic than point contacts. While rolling, the contact force changes direction, as does the respective friction cone. The friction cone *inequality* condition applies as long as the contact is a pure rolling one. Thereby, the tangential accelerations $\dot{v}_{k_t} \in \{\dot{v}_{k_x}, \dot{v}_{k_y}\}$ are zero. At the moment when the friction force reaches the boundary of the cone (i.e. when the inequality in (3.9) changes to equality), the contact joint begins to slide (to accelerate in the tangential direction). This condition is expressed as follows [63]:

$$\mu_k f_{k_z} \dot{v}_{k_t} + f_{k_t} \sqrt{\dot{v}_{k_x}^2 + \dot{v}_{k_y}^2} = 0,\ \ t \in \{x, y\}.$$

### *Soft-Finger Contact Model*

In the field of grasping, soft finger tips are used for better manipulability of the grasped object. With a soft fingertip, torsional moments can be applied. In this case, the point-contact model (3.9) is extended as follows [49]:

$$\left\{ FC_k : \sqrt{f_{k_x}^2 + f_{k_y}^2} \leq \mu_k f_{k_z},\ f_{k_z} \geq 0,\ |m_{k_z}| \leq \gamma_k f_{k_z} \right\}, \tag{3.11}$$

where $\gamma > 0$ is the coefficient of torsional friction.

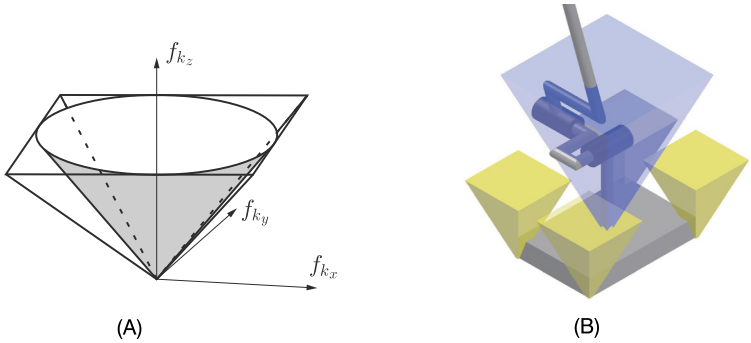


**FIGURE 3.1** Left (A): Approximation of the FC with a circumscribed four-sided pyramid. Right (B): Conceptual graphical representation of polyhedral ($N = 4$) point-contact friction cones (FC, colored in yellow) at the vertices of a rectangular foot and the respective polyhedral plane-contact wrench cone (CWC, colored in purple). The CWC is obtained from the four FCs via face/span transforms.

### *Polyhedral Convex Cone Model*

The above representations of the friction cone are nonlinear. To facilitate analysis and the design of faster numerical algorithms, a linearized representation of the friction cone would be more appropriate. In [63], the friction cone was linearized by approximating it with a friction pyramid. In general, an N-sided convex polyhedron (CP) can be employed [64,32,18], i.e.

$$CP_k = \{\boldsymbol{f}_k : \boldsymbol{C}_k \boldsymbol{f}_k \preceq \boldsymbol{0}\}.$$

The curly inequality sign denotes componentwise operation. We have the matrix

$$\boldsymbol{C}_k = \begin{bmatrix} -\sin\alpha_{1_k} & -\cos\alpha_{1_k} & -\mu_k \\ \vdots & \vdots & \vdots \\ -\sin\alpha_{p_k} & -\cos\alpha_{p_k} & -\mu_k \\ \vdots & \vdots & \vdots \\ -\sin\alpha_{N_k} & -\cos\alpha_{N_k} & -\mu_k \end{bmatrix}, \quad \alpha_{p_k} = \frac{2\pi(p_k - 1)}{N_k}.$$

Increasing $N$ improves the accuracy at the expense of the computational load. In the field of humanoid robotics, mostly used are the four-sided pyramid approximations [47,44,42]. The pyramid can be either inscribed (conservative approach) or circumscribed, as shown in Fig. 3.1A. In this text, the latter approach will be adopted. Then

$$\boldsymbol{C}_k = \begin{bmatrix} 0 & -1 & \mu_k \\ -1 & 0 & \mu_k \\ 0 & 1 & \mu_k \\ 1 & 0 & \mu_k \end{bmatrix}. \tag{3.12}$$

An implementation with a three-sided pyramid approximation can be found in [40].

***Plane-Contact Model: the Contact Wrench Cone***

Consider now the planar-contact joints at the feet. Without friction, only spatial force components $f_z$, $m_x$, and $m_y$ can be transmitted across the joints. As already clarified, normal force $f_z \geq 0$ is transmitted unilaterally while tangential moments $m_x$ and $m_y$ are transmitted bilaterally, with bounds (the meaning of the bounds will be clarified in short). In the presence of friction, these three components determine the hard-constraint directions. The remaining three components (i.e. $f_x$, $f_y$, and $m_z$) will be transmitted as well, either completely (no slipping) or partially (with slipping). These components determine the soft-constraint directions. In other words, the contact model should account for all the six contact wrench components. A "friction cone" that accounts for all the contact wrench components in the general case, i.e. for any type of surface contact, is referred to as a "wrench cone" [3]. As noted in [14], a surface contact can be thought of as a continuum of infinitesimal contact forces encoded locally by a scalar normal pressure field and a 2D vector field for mechanical stress in the tangential directions.

In the particular case of plane contact, the general surface model can be simplified by observing only the contact forces at the vertices of the contact polygon. Consider, for example, the four point contacts at the vertices of a rectangular foot sole, conveniently colocated with existing pressure-type sensors. To ensure friction cone conditions (3.9) at all four point contacts, the components of the wrench cone must satisfy the following constraints [15]:

$$|f_t| \leq \mu f_z, \quad t \in \{x, y\}, \tag{3.13}$$

$$|m_x| \leq l_y f_z, \quad |m_y| \leq l_x f_z, \tag{3.14}$$

$$f_z > 0,$$

$$m_z^{min} \leq m_z \leq m_z^{max}.$$

Here $l_t$ denotes the half-distance between two contact points in the tangential direction $t$. The bounds on yaw moment $m_z$ are determined from

$$m_z^{min} \equiv -\mu(l_x + l_y) f_z + |l_y f_x - \mu m_x| + |l_x f_y - \mu m_y|,$$
$$m_z^{max} \equiv +\mu(l_x + l_y) f_z - |l_y f_x + \mu m_x| - |l_x f_y + \mu m_y|.$$

This model provides valuable information about the admissible bounds on the moment in the vertical direction, which has been shown to play an important role during walking. Note that there is no need to make use of the torsional friction coefficient $\gamma$ with this model.

An important remark is due at this point. The two motion constraints related to the moment components $m_x$ and $m_y$ have been characterized as bilateral since the moments can be transmitted across the planar-contact joint in both directions. However, as seen from (3.14), there are bounds on the absolute values of these moments. These bounds are needed to ensure that the moments do not grow too large. Note that violating this condition yields a change in the type of the contact joint, from plane-type to line-type or point-type. As a consequence of such a change the foot will begin to roll and the moments would cease to be controllable. The respective dual components (i.e. angular speeds $\omega_x$ and/or $\omega_y$) would then become uncontrollable as well, which would in turn cause the robot to lose its stability. Such stability problems will be discussed in more detail in Chapter 5.

The wrench cone for the plane-contact model will be henceforth referred to as the *contact wrench cone* (CWC) [15]. It can be shown that, when the point-contact forces at the vertices are confined within the interior of their friction cones, the contact wrench will be confined within the interior of the CWC [15,14].

***Face/Span Polyhedral Convex Cone Double Representations***

A general procedure for the construction of the CWC can be obtained with the help of the *face/span polyhedral convex cone double representations* [31,3]. The idea is visualized in Fig. 3.1B. With such procedure, it is possible to construct the CWC at a rectangular foot contact, for example, from the polyhedral cones (PCs) at the four vertices.

The face/span representations of a PC are denoted as

$$\begin{aligned} PC &= \text{face}(\boldsymbol{U}) = \{\boldsymbol{f} : \boldsymbol{U}\boldsymbol{f} \preceq \boldsymbol{0}\} \\ &= \text{span}(\boldsymbol{V}) = \{\boldsymbol{V}\boldsymbol{z} : \boldsymbol{z} \succeq \boldsymbol{0}\}. \end{aligned}$$

The face representation can be used to directly check whether a contact force (or wrench) lies within the interior. The span representation, on the other hand, is useful for linear association. Next, note that for a given $\boldsymbol{U}$ there is a $\boldsymbol{U}^S$, s.t. $\text{span}(\boldsymbol{U}^S) = \text{face}(\boldsymbol{U})$. Also, for a given $\boldsymbol{V}$ there is a $\boldsymbol{V}^F$, s.t. $\text{face}(\boldsymbol{V}^F) = \text{span}(\boldsymbol{V})$. Furthermore, denote the force-to-wrench mapping at contact $k$ as

$$\mathcal{F}_k = \mathbb{C}_k \boldsymbol{f}_k.$$

In the case of a rectangular contact area, $\boldsymbol{f}_k \in \Re^{12}$ stands for four stacked point-contact forces and $\mathbb{C}_k \in \Re^{6\times 12}$ is the force-to-wrench map. Assuming that the contact forces are confined within their polyhedral friction cones, i.e. $\boldsymbol{U}_k \boldsymbol{f}_k \preceq \boldsymbol{0}$; it follows then that $\mathcal{F}_k \in \text{span}(\boldsymbol{V}_{k_{CWC}})$, where $\boldsymbol{V}_{k_{CWC}} = \mathbb{C}_k \boldsymbol{U}_k^S$. This implies that the contact wrench lies within the interior of the CWC, i.e. $\boldsymbol{U}_{k_{CWC}} \mathcal{F}_k \preceq \boldsymbol{0}$.

It is worth mentioning that plane-contact models derived from reaction forces at the contact area vertices, as above, are used quite frequently [32,1,34,74,73,68]. Note also that there is an open-source software library for face/span transformations (the CDD library [26]).

### 3.3.3 Motion/Force Duality Relations Across Contact Joints

Contact joints play an important role in humanoid robotics, as already discussed: locomotion depends upon frictional contacts, as does multifinger and dual-arm object manipulation. The motion/force relations across contact joints derived above are based on a fundamental duality property. This property is inherent not only to the contact joints discussed here, but also to any of the robot joints. Moreover, the duality property plays in fact a much broader role and covers motion/force duality relations at the system level.

Consider first the ideal case of a frictionless contact joint. The possible force, $\overline{\mathcal{F}}_k \in \Re^{c_k}$, and the possible motion velocity, $\overline{\mathcal{V}}_k \in \Re^{\eta_k}$, are transmitted across the joint as

$$\mathcal{F}_k = {}^k\mathbb{B}_c \overline{\mathcal{F}}_k \tag{3.15}$$

and

$$\mathcal{V}_k = {}^k\mathbb{B}_m \overline{\mathcal{V}}_k, \tag{3.16}$$

respectively. On the other hand, any spatial force/velocity is suppressed by the joint as

$$ {}^{k}\mathbb{B}_{m}^{T}\mathcal{F}_{k} = \mathbf{0} \tag{3.17} $$

and

$$ {}^{k}\mathbb{B}_{c}^{T}\mathcal{V}_{k} = \mathbf{0}, \tag{3.18} $$

respectively. Since ${}^{k}\mathbb{B}_{c} \in \Re^{6\times c_k}$ and ${}^{k}\mathbb{B}_{m} \in \Re^{6\times \eta_k}$ are full column rank by definition, there exist respective complementary matrices ${}^{k}\mathbb{B}_{c}^{\perp} \in \Re^{6\times \eta_k}$ and ${}^{k}\mathbb{B}_{m}^{\perp} \in \Re^{6\times c_k}$, s.t.

$$ {}^{k}\mathbb{B}_{c}^{\perp} = {}^{k}\mathbb{B}_{m}, \;\; {}^{k}\mathbb{B}_{m}^{\perp} = {}^{k}\mathbb{B}_{c}, \tag{3.19} $$

where $(\circ)^{\perp} = \boldsymbol{E} - (\circ)$ denotes the orthogonal complement. The pairs $\{{}^{k}\mathbb{B}_{c}, \; {}^{k}\mathbb{B}_{c}^{\perp}\}$ and $\{{}^{k}\mathbb{B}_{m}, \; {}^{k}\mathbb{B}_{m}^{\perp}\}$ span the spatial force and motion subspaces, respectively (cf. also [60], Section 2.4.4). Note also that the direct sum ${}^{k}\mathbb{B}_{c} \oplus {}^{k}\mathbb{B}_{m} = \boldsymbol{E}_{6}$.

Next, consider a joint with friction. Recall that such a joint is fully constrained, whereby the hard constraints (inadmissible motion) are distinguished from the soft ones, the latter admitting motion under friction. The respective constraint directions are determined by the basis vector matrices defined for frictionless joints. Denote by $\overline{\mathcal{F}}_{k}^{h} \in \Re^{c_k^h}$ and $\overline{\mathcal{F}}_{k}^{s} \in \Re^{c_k^s}$ the friction wrench components transmitted along the hard and soft constraint directions, respectively. Furthermore, a damped velocity component, $\overline{\mathcal{V}}_{k}^{s} \in \Re^{c_k^s}$, may be transmitted across the joint while sliding, in accordance with (3.10). From the complementarity relations (3.19) it follows that the friction wrench and the damped velocity components along the soft-constraint directions are transformed within the respective spatial force/velocity domains as

$$ \mathcal{F}_{k} = {}^{k}\mathbb{B}_{m}\overline{\mathcal{F}}_{k}^{s} \tag{3.20} $$

and

$$ \mathcal{V}_{k} = {}^{k}\mathbb{B}_{c}\overline{\mathcal{V}}_{k}^{s}, \tag{3.21} $$

respectively. On the other hand, any wrench acting on the link adjacent to the joint induces the following force component in the soft-constraint directions:

$$ \overline{\mathcal{F}}_{k}^{s} = {}^{k}\mathbb{B}_{m}^{T}\mathcal{F}_{k}. \tag{3.22} $$

Note that $\overline{\mathcal{F}}_{k}^{h}$ and $\overline{\mathcal{F}}_{k}^{s}$ have to be evaluated for compliance with the friction cone condition. When the condition is violated, the joint begins to slide and the dynamic friction model (3.10) comes into effect. The components of the velocity in the mobility directions are obtained via the transform

$$ \overline{\mathcal{V}}_{k}^{s} = {}^{k}\mathbb{B}_{c}^{T}\mathcal{V}_{k}. \tag{3.23} $$

The above duality relations are represented graphically in Fig. 3.2. For a frictionless joint, the joint-motion constraint yields the impossible motion/force subspaces. In the case of a joint with friction, these subspaces become the friction-force and the damped-motion (friction-induced damping) subspaces, respectively.

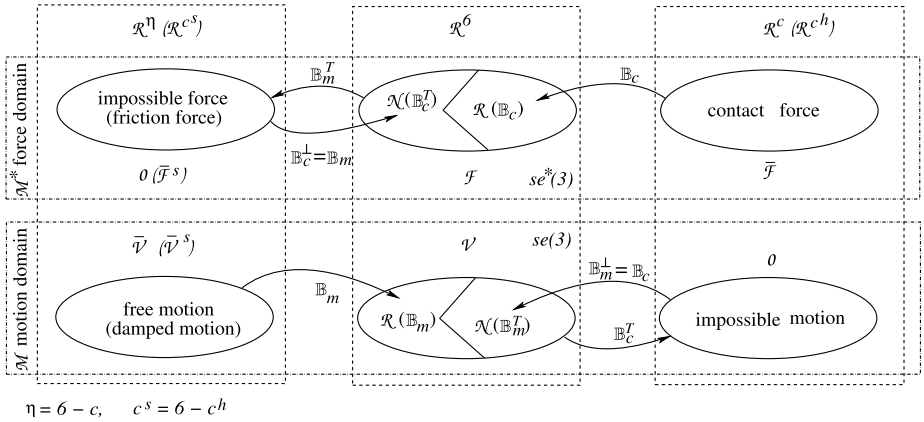


**FIGURE 3.2** Motion/force duality relations across a contact joint. The 6D parameter space of motion/force domains $se(3)/se^*(3)$ is decomposed as $\Re^6 = \Re^c \oplus \Re^\eta$ (frictionless joint) or $\Re^6 = \Re^{c^h} \oplus \Re^{c^s}$ (joint with friction). The right angles in the $\Re^6$ subdomains represent orthogonal decomposition. Note that $\mathcal{R}(\mathbb{B}_m) = \mathcal{N}(\mathbb{B}_c^T)$ and vice versa. A frictionless joint comprises the *impossible-force* and the *free-motion* complementary subspaces. For a joint with friction, these subspaces become the *friction-force* and the friction-induced *damped-motion* subspaces, respectively.

### *Summary and Discussion*

The *constraint-based* contact modeling method presented here refers to contact joints between rigid bodies. A contact joint may impose constraints characterized with or without friction. There are $c_k \leq 6$ motion constraints enforced by the contact joint. In the presence of friction, the contact joint model is determined by the pair $\{\mathbb{B}_c, FC_k\}$; $\mathbb{B}_c$ denotes the constraint basis for independent wrench components across the joint and $FC_k$ stands for the friction cone that plays an important role in assessing the state of the frictional constraints. Most of the research in the field of humanoid robotics assumes that the *reaction* force at the contact is always positive or nonnegative. This is in contrast with the contact models used in the field of multifinger grasping [49] where the forces *impressed* by the fingers on the object are assumed positive.[1]

Constraint-based modeling is useful in motion/force analysis of constrained multibody systems like human figures in animation and humanoid robots. The implementation of the method in numerical environments for simulation and control, however, is not straightforward. For example, note that the friction cone (3.9) represents a system of nonlinear inequalities. When modeling frictional contacts numerically, the friction cone can be approximated by a pyramid [63] or by a convex PC for improved accuracy [31,62,3]. The problem can then be cast and solved as a linear complementarity problem (LCP) [5,62,2]. The respective standard solution methods lead to complexity, though, when applied to a multi-DoF system like a humanoid robot. Other problematic issues also exist. The related problems have been tackled via alternative modeling methods [39,51,17,70].

[1] These forces always point outward from the fingertips; see also [63].

## 3.4 KINETOSTATIC RELATIONS IN INDEPENDENT CLOSED-LOOP CHAINS

In Section 2.10 it was shown how important it is to determine instantaneous motion relations for kinematic chains comprising closed loops. The dual problem of determining *kinetostatic* forces within the closed loops is of equal significance. Such forces appear in multifinger grasping, dual-arm cooperating manipulation, and legged robots, including humanoids. The differential kinematic and kinetostatic force relations are complementary relations stemming from d'Alembert's principle of virtual work. The relations are obtained under the assumption of locked joints, s.t. $\dot{\boldsymbol{\theta}} = \mathbf{0}$ always.

Consider the case of two independent closed loops, as described in Section 2.10.1 (see also Fig. 3.6). Each closed loop is formed by the two contact joints at the respective end links. The force/moment relations within each closed loop are determined by the external wrenches acting at one or more of the links within the loop, the gravity field, and the joint torque vectors of the two limbs, $\boldsymbol{\tau}_k,\ k \in \{e_r,\ e_l\}$. The external wrench $-\mathcal{F}_\lambda$ acting on Link $\lambda$ can be expressed as the following sum:

$$\mathcal{F}_\lambda = \sum_k \mathbb{T}^T_{\underleftarrow{\lambda k}}(\boldsymbol{q}_e)\mathcal{F}_k^{\ \lambda}. \tag{3.24}$$

Wrench $\mathcal{F}_k^{\ \lambda}$ is the contact wrench at contact joint $k$ stemming from the external wrench $\mathcal{F}_\lambda$. By convention, the minus sign signifies that external wrenches are treated as being *impressed* by the robot on the environment. A positive wrench has then the meaning of a *reaction wrench*, in accordance with Newton's Third Law. Further on, the actions of all external wrenches, $\mathcal{F}_k^{\ \lambda}$ $(\lambda = 1, 2, ...)$, sum up at contact joint $k$ as the *total contact wrench*, i.e. $\mathcal{F}_k = \sum_\lambda \mathcal{F}_k^{\ \lambda}$. On the other hand, the sum of all external wrenches, taken at the root link, determines the reaction to the net external wrench within the loop, i.e.

$$\mathcal{F}_R = \sum_\lambda \mathbb{T}^T_{\underleftarrow{R\lambda}}(\boldsymbol{q}_e)\mathcal{F}_\lambda = \sum_k \mathbb{T}^T_{\underleftarrow{Rk}}(\boldsymbol{q}_k)\mathcal{F}_k. \tag{3.25}$$

The term $\mathcal{F}_R$ will be henceforth referred to as the *root wrench*. A similar relation is used to map the sum of all external wrenches at the loop-closure link:

$$\mathcal{F}_e = \sum_\lambda \mathbb{T}^T_{\underleftarrow{e\lambda}}(\boldsymbol{q}_e)\mathcal{F}_\lambda = \sum_k \mathbb{T}^T_{\underleftarrow{ek}}(\boldsymbol{q}_k)\mathcal{F}_k. \tag{3.26}$$

The term $\mathcal{F}_e$ will be henceforth referred to as the *closure-link wrench*. Note that the above maps can be characterized as configuration-dependent *structural force* maps.

Finally, to ensure the closure of the loop, the total contact wrench $\mathcal{F}_k$ should be in balance with the contact wrench stemming from the joint torque of the respective limb. This implies that

$$\boldsymbol{\tau}_k = \boldsymbol{J}_R^T(\boldsymbol{q}_k)\,\mathcal{F}_k. \tag{3.27}$$

This relation is valid for a nonredundant limb. In the case of a kinematically redundant limb, a null-space term has to be added, as will be clarified shortly.

### 3.4.1 Orthogonal Decomposition of the Contact Wrench

The contact wrench $\mathcal{F}_k$ can be decomposed along the constrained ($c$) and unconstrained/mobility ($m$) directions in accordance with the relations discussed in Section 2.9. We have

$$\begin{aligned}\mathcal{F}_k &= \mathcal{F}_k^c + \mathcal{F}_k^m \\ &= \mathbb{B}_c(\boldsymbol{q}_k)\overline{\mathcal{F}}_k^c + \mathbb{B}_m(\boldsymbol{q}_k)\overline{\mathcal{F}}_k^m \\ &= \left[(\overline{\mathcal{F}}_k^c)^T \quad (\overline{\mathcal{F}}_k^m)^T\right]^T.\end{aligned} \tag{3.28}$$

The two wrenches in the sum are orthogonal, i.e. $\mathcal{F}_k^c \perp \mathcal{F}_k^m$. Component $\overline{\mathcal{F}}_k^c \in \Re^{c_k}$ denotes the *reactions* along the constrained directions at the contact joint; $\overline{\mathcal{F}}_k^m \in \Re^{\eta_k}$ stands for *inertial* force/moment components in the unconstrained directions. Thus, the above relations are of a *kinetostatic* nature.

The notation covers the two special cases of completely constrained or completely unconstrained motion, i.e. $c_k = 6$, $\eta_k = 0$, $\mathcal{F}_k = \mathcal{F}_k^c$ and $c_k = 0$, $\eta_k = 6$, $\mathcal{F}_k = \mathcal{F}_k^m$, respectively. The latter is trivial from the viewpoint of statics. The completely constrained case, on the other hand, deserves more attention in view of friction modeling and control. The friction models introduced in Section 3.3.2 can be employed, e.g. as defined in (3.9) or (3.13) for the cases of point or plane contacts, respectively. It is assumed that proper control is available (cf. Chapter 5) s.t. the contact wrench is always confined within the interior of the friction cone ($FC_k$: point contact) or the contact wrench cone ($CWC_k$: line or plane contact). This implies that the contact joint never *slips* and thus imposes a complete motion constraint. In this case, the reaction/contact wrench can be decomposed as

$$\begin{aligned}\mathcal{F}_k &= \mathcal{F}_k^c = \mathcal{F}_k^h + \mathcal{F}_k^s \\ &= \mathbb{B}_c(\boldsymbol{q}_k)\overline{\mathcal{F}}_k^h + \mathbb{B}_m(\boldsymbol{q}_k)\overline{\mathcal{F}}_k^s \\ &= \left[(\overline{\mathcal{F}}_k^h)^T \quad (\overline{\mathcal{F}}_k^s)^T\right]^T.\end{aligned} \tag{3.29}$$

The $h$ and $s$ superscripts refer to the normal and tangential directions at the contact joint. This decomposition is of the same form as (3.28). However, the meaning of the two components, $\overline{\mathcal{F}}_k^h$ and $\overline{\mathcal{F}}_k^s$, is different; they both are *reactions*. Thus, the above relations are characterized as pure static relations. An illustrative example will be presented in Section 3.6.5.

### 3.4.2 Orthogonal Decomposition of the Loop-Closure and Root Link Wrenches

Decomposition (3.28) of each contact wrench induces the following decomposition of the wrench at the loop-closure link:

$$\begin{aligned}\mathcal{F}_e &= \mathcal{F}_e^c + \mathcal{F}_e^m \\ &= \sum_k \mathbb{C}_{ce}(\boldsymbol{q}_k)\overline{\mathcal{F}}_k^c + \sum_k \mathbb{C}_{me}(\boldsymbol{q}_k)\overline{\mathcal{F}}_k^m \\ &= \mathbb{C}_{ce}(\boldsymbol{q}_e)\overline{\mathcal{F}}^c(\boldsymbol{q}_e) + \mathbb{C}_{me}(\boldsymbol{q}_e)\overline{\mathcal{F}}^m(\boldsymbol{q}_e),\end{aligned} \tag{3.30}$$

$\overline{\mathcal{F}}^{(\circ)}(\boldsymbol{q}_e)$ denoting vectors of stacked $\overline{\mathcal{F}}_k^{(\circ)}$ components. Note that from the definition of the contact maps it follows that $\mathcal{F}_e^c \perp \mathcal{F}_e^m$. The importance of this loop-closure wrench decomposition will also be highlighted with an example in Section 3.6.5.

The root-link wrench is decomposed in the same way: in the above relations just replace contact map $\mathbb{C}_{(\circ)e}$ with $\mathbb{C}_{(\circ)R}$.

### 3.4.3 Decomposition of the Limb Joint Torque

The joint torque of Limb $k$, (3.27), will be decomposed into components stemming from the contact wrenches along the constrained and mobility directions, as follows. First, a relation dual to the first-order differential motion constraint (i.e. the upper part of (2.73)) will be derived via d'Alembert's principle of virtual work. Denote by $\delta\boldsymbol{\theta}_k$ and $\delta\mathcal{X}_k^c$ the virtual joint displacements and the relative virtual displacements at the contacts, respectively, the latter being associated with $\overline{\mathcal{V}}_k^c - \mathbb{C}_{cR}(\boldsymbol{q}_k)\mathcal{V}_R$. The virtual displacements can be related as $\mathcal{J}_{cR}(\boldsymbol{q}_k)\delta\boldsymbol{\theta}_k = \delta\mathcal{X}_k^c$. The instantaneous virtual work can then be expressed as

$$\delta\boldsymbol{\theta}_k^T\boldsymbol{\tau}_k^c = (\delta\mathcal{X}_k^c)^T\overline{\mathcal{F}}_k^c = \delta\boldsymbol{\theta}_k^T\mathcal{J}_{cR}^T(\boldsymbol{q}_k)\overline{\mathcal{F}}_k^c.$$

This relation is valid for any $\delta\boldsymbol{\theta}_k$. Thus, one obtains the joint torque component stemming from the contact wrench along the constrained-motion directions as

$$\boldsymbol{\tau}_k^c = \mathcal{J}_{cR}^T(\boldsymbol{q}_k)\overline{\mathcal{F}_k}^c. \tag{3.31}$$

The complementary quasistatic relationship can be obtained in a similar way from the lower part of (2.73) as

$$\boldsymbol{\tau}_k^m = \mathcal{J}_{mR}^T(\boldsymbol{q}_k)\overline{\mathcal{F}_k}^m. \tag{3.32}$$

The sum of the last two equations is

$$\boldsymbol{\tau}_k = \boldsymbol{\tau}_k^c + \boldsymbol{\tau}_k^m = \begin{bmatrix}\mathcal{J}_{cR}^T(\boldsymbol{q}_k) & \mathcal{J}_{mR}^T(\boldsymbol{q}_k)\end{bmatrix}\begin{bmatrix}\overline{\mathcal{F}}_k^c \\ \overline{\mathcal{F}}_k^m\end{bmatrix} = \mathcal{J}_R^T(\boldsymbol{q}_k)\mathcal{F}_k. \tag{3.33}$$

Jacobian $\mathcal{J}_R(\boldsymbol{q}_k)$ is the permuted Jacobian of the limb (cf. (2.77)). The above result is in agreement with the decomposition of the total wrench at the contact joint, as in (3.28), and the expression for the limb joint torque in (3.27). Note that the above decomposition is *not* orthogonal.

In the case of a kinematically redundant limb, the joint torque can be expressed as [38]

$$\boldsymbol{\tau}_k = \mathcal{J}_R^T(\boldsymbol{q}_k)\mathcal{F}_k + \left(\boldsymbol{E} - \mathcal{J}_R^T(\boldsymbol{q}_k)\mathcal{J}_R^{\#T}(\boldsymbol{q}_k)\right)\boldsymbol{\tau}_{k_u}. \tag{3.34}$$

The homogeneous component of the joint torque (the second component on the r.h.s.) induces self-motion via the vector parameter $\boldsymbol{\tau}_{k_u}$. A special subset of self-motion can be determined via an appropriated choice of the generalized inverse (cf. Section 4.5.2), s.t. the force balance at the end link, and hence the static contact conditions within the closed loop can be maintained; $\left(\boldsymbol{E} - \mathcal{J}_R^T(\boldsymbol{q}_k)\mathcal{J}_R^{\#T}(\boldsymbol{q}_k)\right)$ is a projector onto the dual null space of the limb Jacobian,

$\mathcal{N}\left(\mathcal{J}_R^{\#T}(\boldsymbol{q}_k)\right)$. This null space is identical with the intersection of the dual null spaces of the two sub-Jacobians in (3.33), i.e.

$$\mathcal{N}^*\big(\mathcal{J}_R(\boldsymbol{q}_k)\big) = \mathcal{N}^*\big(\mathcal{J}_{cR}(\boldsymbol{q}_k)\big) \cap \mathcal{N}^*\big(\mathcal{J}_{mR}(\boldsymbol{q}_k)\big)\,.$$

The asterisk superscript signifies that the dual null space is defined within the joint torque (force) domain, i.e.,

$$\mathcal{N}^*(\boldsymbol{A}) \equiv \mathcal{N}(\boldsymbol{A}^{\#T}). \tag{3.35}$$

Assuming a weighted generalized inverse, as in (2.41), it is straightforward to show that the null-space projector in the force domain is related to the null-space projector in the motion domain (as in (2.34) and (2.39)), via the following similarity transform:

$$\boldsymbol{W}^{-1}\left(\boldsymbol{E} - \boldsymbol{A}^T\boldsymbol{A}^{-WT}\right)\boldsymbol{W} = \left(\boldsymbol{E} - \boldsymbol{A}^{-W}\boldsymbol{A}\right). \tag{3.36}$$

The last equation implies that the two null spaces are isomorphic, i.e. $\mathcal{N}(\boldsymbol{A}) \simeq \mathcal{N}(\boldsymbol{A}^{\#T})$ and the respective (dual) vector bases are of the same dimension and of equal rank. Given a null-space projector, $\boldsymbol{N}(\circ)$, the dual projector will be denoted as $\boldsymbol{N}^*(\circ)$.

Further on, to honor the priority convention (2.86) of the velocity solution, the limb joint torque (3.34) can be rewritten as

$$\begin{aligned}\boldsymbol{\tau}_k &= \mathcal{J}_{cR}{}^T(\boldsymbol{q}_k)\overline{\mathcal{F}}_k^c + \overline{\mathcal{J}}_{mR}(\boldsymbol{q}_k)\widetilde{\mathcal{F}}_k^m + \left(\boldsymbol{E} - \mathcal{J}_R^T(\boldsymbol{q}_k)\mathcal{J}_R^{\#T}(\boldsymbol{q}_k)\right)\boldsymbol{\tau}_{k_u}, \\ &= \boldsymbol{\tau}_k^c + \boldsymbol{\tau}_k^m + \boldsymbol{\tau}_k^n, \;\text{ s.t. } \boldsymbol{\tau}_k^c \succ \boldsymbol{\tau}_k^m \succ \boldsymbol{\tau}_k^n.\end{aligned} \tag{3.37}$$

Here $\overline{\mathcal{J}}_{mR}(\boldsymbol{q}_k) = \mathcal{J}_{mR}(\boldsymbol{q}_k)\boldsymbol{N}^*(\mathcal{J}_{cR}(\boldsymbol{q}_k))$ is the mobility Jacobian restricted by the dual null space of the joint-space constraint Jacobian, and $\widetilde{\mathcal{F}}_k^m = \overline{\mathcal{F}}_k^m - \mathcal{J}_{mR}^{\#T}(\boldsymbol{q}_k)\mathcal{J}_{cR}^T(\boldsymbol{q}_k)\overline{\mathcal{F}}_k^n$. The torque component $\boldsymbol{\tau}_k^c$ ensures that the reaction forces at the contact are maintained with the highest priority; $\boldsymbol{\tau}_k^m$, on the other hand, is used as a control input w.r.t. the forces along the unconstrained motion directions at the contact (friction or inertial forces). Finally, $\boldsymbol{\tau}_k^n$ can be used for self-motion control, as explained above.

Eq. (3.34) plays an important role in the inverse dynamic relations of redundant manipulators. Further details will be provided in Section 4.5.

## 3.5 THE WRENCH DISTRIBUTION PROBLEM

The kinetostatic relations derived in the last section state that the contact wrench components at the loop contact joints determine the root and closure-link wrenches, $\mathcal{F}_R$ and $\mathcal{F}_e$, respectively. The inverse problem, i.e. "Given the root (or closure-link) wrench, find appropriate reactions at the contact joints," plays an important role in balance, propulsion, and cooperative (dual-arm) manipulation control. Indeed, the only way to control a free-floating root link, such as the base link of a humanoid robot, is to generate appropriate reactions at the contact joints. The inverse problem is referred to as the *wrench distribution* (WD) problem.

In what follows, the WD problem will be explained with regard to the loop-closure link. The same relations can be used for the WD problem with regard to the root link, by replacement of the contact maps. First, it is important to note that the WD problem is a pure static problem. The total *reaction* wrench lumped at the loop-closure link is $\mathcal{F}_e = \mathcal{F}_e^c$. As already clarified, the other component of $\mathcal{F}_e$ appearing in (3.30), $\mathcal{F}_e^m$, stems from inertia forces along the mobility directions at frictionless contacts and, hence, should not appear in the static balance of forces. Thus, from (3.30), we obtain

$$\begin{aligned} \mathcal{F}_e &= \mathbb{C}_{ce}(\boldsymbol{q}_e)\,\overline{\mathcal{F}}^c(\boldsymbol{q}_e), \\ \overline{\mathcal{F}}^c(\boldsymbol{q}_e) &= \left[(\overline{\mathcal{F}}_{e_r}^c)^T \quad (\overline{\mathcal{F}}_{e_l}^c)^T\right]^T \in \Re^{c_e}. \end{aligned} \tag{3.38}$$

This notation also covers contact joints with friction, whereby $\overline{\mathcal{F}}_{e_j}^c = \mathcal{F}_{e_j}^c = \mathcal{F}_{e_j}$, for $j = r$ or $j = l$ or both. In the latter case, $\overline{\mathcal{F}}^c(\boldsymbol{q}_e) = \mathcal{F}^c(\boldsymbol{q}_e) = \mathcal{F}(\boldsymbol{q}_e) \in CWC_e$ should hold, where

$$CWC_e = CWC_{e_r} \times CWC_{e_l} \subset \Re^{12}$$

is the *loop CWC*.

### 3.5.1 General Solution to the Wrench Distribution Problem

The solution to the inverse problem may not be a trivial one since the conditioning of the linear system (3.38) depends on the type and number of constraints, their independence, and the configuration of the limbs. To satisfy the loop-closure conditions, the composite wrench $\overline{\mathcal{F}}^c(\boldsymbol{q}_e)$ should ensure contact stability and comply with the above CWC constraints. This implies the involvement of *inequality-type constraints*. In the general case, the loop-closure/root links are *unilaterally overconstrained* ($c_e > 6$), e.g. as in a double-stance posture with high friction. The inverse problem is then underdetermined, admitting an infinite number of solutions. This is also the case for an object held by the hands. Thus

$$\overline{\mathcal{F}}^c(\boldsymbol{q}_e) = \mathbb{C}_{ce}^{\#}(\boldsymbol{q}_e)\mathcal{F}_e + \overline{\mathcal{F}}^n(\boldsymbol{q}_e), \tag{3.39}$$

$$\overline{\mathcal{F}}^n(\boldsymbol{q}_e) = \boldsymbol{N}\left(\mathbb{C}_{ce}(\boldsymbol{q}_e)\right)\overline{\mathcal{F}}_a^c(\boldsymbol{q}_e) \tag{3.40}$$

$$= \boldsymbol{V}\left(\mathbb{C}_{ce}(\boldsymbol{q}_e)\right)\overline{\mathcal{F}}^{int}(\boldsymbol{q}_e). \tag{3.41}$$

The form of this solution is similar to the inverse kinematics solution of a kinematically redundant limb (cf. (2.34)), comprising particular and homogeneous solution components. The former is composed of contact wrench components that compensate the action of the closure-link wrench $\mathcal{F}_e$. The contact wrench component $\overline{\mathcal{F}}^n(\boldsymbol{q}_e) \in \mathcal{N}\left(\mathbb{C}_{ce}(\boldsymbol{q}_e)\right)$, on the other hand, being derived from the null space of the loop contact map, does not alter the wrench balance at the closure link; $\overline{\mathcal{F}}^n(\boldsymbol{q}_e)$ will be referred to as the *null-space contact wrench component*. Note that in (3.40) and (3.41), the null space is parametrized nonminimally/minimally by $\overline{\mathcal{F}}_a^c(\boldsymbol{q}_e)$ and $\overline{\mathcal{F}}^{int}(\boldsymbol{q}_e) \in \Re^{c_e-6}$, respectively.

### 3.5.2 Internal Force/Moments: the Virtual Linkage Model

The null-space contact wrench component $\overline{\mathcal{F}}^n$ is related to the *internal force/moments* within the closed loop. The internal force was first introduced in the field of multifinger grasping [58]. The components of the internal force do not contribute to the displacement of the grasped object; they can be used to squeeze it, and at the same time to ensure the friction and the joint-torque limit constraints [37,50]. In [43], the components of the internal force (referred to as the "interaction forces") were interpreted as pairs of equal and opposite forces acting along the lines joining the contact points. The internal force also plays an important role in the field of object manipulation by dual-arm and cooperating robots. In this case, bilateral contacts are quite often assumed [75,65,69]. Then the compressive and tension forces can both be controlled via the components of the internal force. In addition, *internal moments* can be controlled as well. The internal force/moments play an important role in humanoid robotics with regard to such subtasks as balance control under multiple contacts (e.g. with a double-stance posture), motion/force control, and object manipulation with a multifinger hand, a dual-arm robot, or cooperatively by multiple robots, as well as whole-body pushing [27,57,59,35,48].

The physical meaning of the internal force/moments will be clarified below with the help of the *Virtual Linkage* (VL) model [69].

#### *Internal Forces*

Assume that $p$ *completely constrained* contact joints are formed at closure link $\{e\}$. Combining the contact joint pairs, one obtains the number ${}_pC_2 = p(p-1)/2$. In the case of point contacts, it is sufficient to consider only force components. The wrench impressed by the contact forces upon the loop closure link is defined as $\mathcal{F}_{e_f} = \begin{bmatrix} \boldsymbol{f}_e^T & \boldsymbol{m}_e^T \end{bmatrix}^T$. It can be expressed as

$$\mathcal{F}_{e_f} = \sum_k \mathbb{S}_L \mathbb{T}_{\overleftarrow{ek}}^T \boldsymbol{f}_k = \mathbb{T}_f^T \boldsymbol{f}^c;$$

$\mathbb{S}_L$ extracts the left column of $\mathbb{T}_{\overleftarrow{ek}}^T$, and $\boldsymbol{f}^c \in \Re^{3p}$ and $\mathbb{T}_f^T \in \Re^{6\times 3p}$ are composed of stacked $\boldsymbol{f}_k$ and $\mathbb{S}_L \mathbb{T}_{\overleftarrow{ek}}^T$ components, respectively. The solution to the WD problem can then be written as

$$\boldsymbol{f}^c = (\mathbb{T}_f^T)^{\#} \mathcal{F}_{e_f} + \boldsymbol{N}(\mathbb{T}_f^T) \boldsymbol{f}_a^c. \tag{3.42}$$

Note that the null space $\mathcal{N}(\mathbb{T}_f^T)$ is nonminimally parametrized by $\boldsymbol{f}_a^c \in \Re^{3p}$.

As an example, consider a closed loop with four bilateral point contacts, as shown in Fig. 3.3. According to the VL model, the pairs of forces between the contacts are represented by linearly actuated members that can apply compression/tension force components. With $p = 4$ the number of internal forces is ${}_pC_2 = 6$. The internal forces, denoted as $f_{ij}^{int}$ $\left(i, j \in \{\overline{1,4}\},\ i \neq j\right)$, act along the links of the VL model determined by unit vectors (cf. Fig. 3.3A)

$$\boldsymbol{e}_{ij} = \frac{\boldsymbol{r}_j - \boldsymbol{r}_i}{|\boldsymbol{r}_j - \boldsymbol{r}_i|},\ \boldsymbol{e}_{ij} = -\boldsymbol{e}_{ji},$$

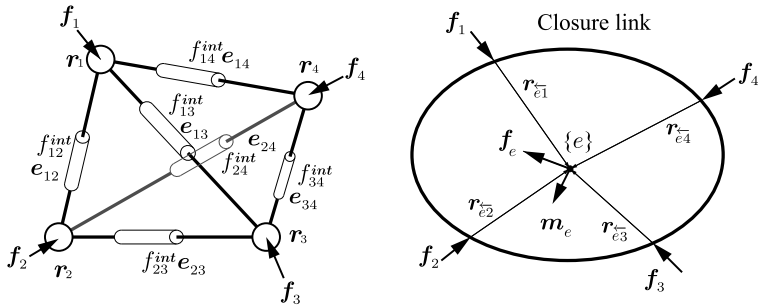


**FIGURE 3.3** Virtual linkage model [69] for a closed loop with four bilateral point contacts. (A) Contact forces and tension/compression forces at the virtual links. (B) Resultant force/moment impressed at the center of frame $\{e\}$ on the loop-closure link.

$\boldsymbol{r}_{(\circ)}$ denoting the positions of the contact joints. The contact force components stemming from the internal forces can then be determined as

$$\begin{bmatrix} \boldsymbol{f}_1^n \\ \boldsymbol{f}_2^n \\ \boldsymbol{f}_3^n \\ \boldsymbol{f}_4^n \end{bmatrix} = \begin{bmatrix} \boldsymbol{e}_{12} & \boldsymbol{e}_{13} & \boldsymbol{e}_{14} & \boldsymbol{0} & \boldsymbol{0} & \boldsymbol{0} \\ \boldsymbol{e}_{21} & \boldsymbol{0} & \boldsymbol{0} & \boldsymbol{e}_{23} & \boldsymbol{e}_{24} & \boldsymbol{0} \\ \boldsymbol{0} & \boldsymbol{e}_{31} & \boldsymbol{0} & \boldsymbol{e}_{32} & \boldsymbol{0} & \boldsymbol{e}_{34} \\ \boldsymbol{0} & \boldsymbol{0} & \boldsymbol{e}_{41} & \boldsymbol{0} & \boldsymbol{e}_{42} & \boldsymbol{e}_{43} \end{bmatrix} \begin{bmatrix} f_{12}^{int} \\ f_{13}^{int} \\ f_{14}^{int} \\ f_{23}^{int} \\ f_{24}^{int} \\ f_{34}^{int} \end{bmatrix}. \tag{3.43}$$

The above equation is represented in compact form as

$$\boldsymbol{f}^n = \boldsymbol{V}_L \boldsymbol{f}^{int}, \tag{3.44}$$

where $\boldsymbol{f}^{int} \in \Re^{pC_2}$ and $\boldsymbol{V}_L \in \Re^{3p \times pC_2}$. The vector $\boldsymbol{f}^n \in \Re^{3p}$ is composed of the stacked contact force components $\boldsymbol{f}_k^n$. Note that this set of contact forces do not contribute to the closure-link wrench, i.e. this is a *null-space contact force component*. The solution to the WD problem (3.42) can then be rewritten as

$$\boldsymbol{f}^c = (\mathbb{T}_f^T)^{\#} \mathcal{F}_e + \boldsymbol{f}^n(\boldsymbol{f}^{int}).$$

Hereby, null space $\mathcal{N}^*(\mathbb{T}_f^T)$ is minimally parametrized by the internal force vector $\boldsymbol{f}^{int}$. It then becomes apparent that $\boldsymbol{V}_L$ is a mapping onto that null space, s.t. $\mathbb{T}_f^T \boldsymbol{V}_L \equiv \boldsymbol{0}_6$ holds.

### *Internal Moments*

Consider now the case of plane contacts in 3D that can impress moment components upon the loop-closure link. These components represent in fact the internal moments within the closed loop. In the case of independent contact constraints, three internal moments will be

generated at each contact joint [69]. The following relations can be established:

$$\begin{aligned} \boldsymbol{m}_k &= \boldsymbol{m}_k^{int}, \\ \boldsymbol{m}_e &= \sum_k \boldsymbol{m}_k, \\ \boldsymbol{m}^{int} &= \boldsymbol{m}^n \in \Re^{3p}, \end{aligned} \tag{3.45}$$

where $\boldsymbol{m}^{int}$ is composed of the stacked $\boldsymbol{m}_k^{int}$ components.

***Internal Wrench***

By definition, the sum of the contact wrench components stemming from the internal force/moment vectors do not alter the wrench balance at the loop-closure and root links, i.e.

$$\mathbb{T}_f^T \boldsymbol{f}^n + \mathbb{T}_m^T \boldsymbol{m}^n = \boldsymbol{0}. \tag{3.46}$$

Combining the force/moment relations derived so far, one obtains the system

$$\begin{bmatrix} \boldsymbol{0}_6 \\ \boldsymbol{f}^{int} \\ \boldsymbol{m}^{int} \end{bmatrix} = \begin{bmatrix} \mathbb{T}_f^T & \mathbb{T}_m^T \\ \boldsymbol{V}_L^+ & \boldsymbol{0}_{{}_pC_2 \times 3p} \\ \boldsymbol{0}_{3p} & \boldsymbol{E}_{3p} \end{bmatrix} \begin{bmatrix} \boldsymbol{f}^n \\ \boldsymbol{m}^n \end{bmatrix}. \tag{3.47}$$

The matrix $\mathbb{T}_m^T \in \Re^{6 \times 3p}$ is defined by the following relation:

$$\mathcal{F}_{e_m} = \begin{bmatrix} \boldsymbol{0} \\ \boldsymbol{m}_e \end{bmatrix} = \mathbb{T}_m^T \boldsymbol{m}^n.$$

Apparently, the first three rows of $\mathbb{T}_m^T \in \Re^{6 \times 3p}$ are zeros. The last three must be ones, in accordance with (3.45). Furthermore, note that the second equation in (3.47) stems from the approximate (least-squares) resolution of internal forces in (3.44), $\boldsymbol{V}_L^+$ denoting the *left* pseudoinverse. Note also that, according to that equation, contact moments $\boldsymbol{m}^n$ make no contribution to $\boldsymbol{f}^{int}$. It becomes then apparent that the above resolution of the internal forces is not an exact one. As noted in [69], such approximation is admissible under the assumption that the internal moments will be minimized, as is often the case in humanoid robotics. System (3.47) can be written in compact form as

$$\mathcal{F}^{int} = \boldsymbol{G} \mathcal{F}^n, \tag{3.48}$$

where $\boldsymbol{G} \in \Re^{(3p + {}_pC_2) \times 6p}$ is referred to as the *grasp description matrix* (GDM) [69].

For control purposes, the contact wrenches need to be determined. Assuming that the internal force/moments are known, the respective contact wrench components can be obtained from (3.48) and (3.47) as

$$\mathcal{F}^n = \boldsymbol{G}^{-1} \mathcal{F}^{int}, \tag{3.49}$$

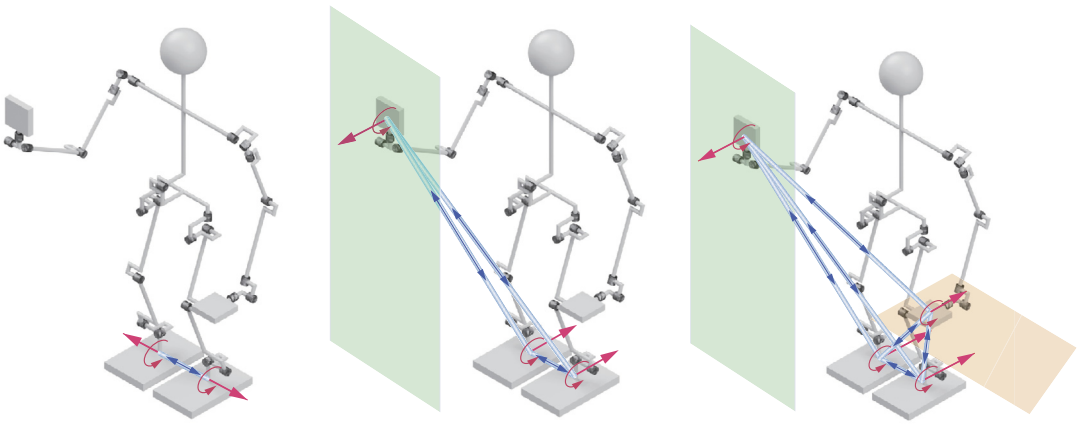


**FIGURE 3.4** Virtual linkages for two (A), three (B), and four (C) plane contacts. The blue and the red arrows indicate the internal forces and the contact wrenches, respectively.

$$\begin{bmatrix} \boldsymbol{f}^n \\ \boldsymbol{m}^n \end{bmatrix} = \begin{bmatrix} (\mathbb{T}_f^T)^+ & \boldsymbol{V}_L & -(\mathbb{T}_f^T)^+ \mathbb{T}_m^T \\ (\mathbb{T}_m^T)^+ & \mathbf{0}_{3p \times {}_pC_2} & \boldsymbol{E}_{3p} \end{bmatrix} \begin{bmatrix} \mathbf{0} \\ \boldsymbol{f}^{int} \\ \boldsymbol{m}^{int} \end{bmatrix}$$
$$= \begin{bmatrix} \boldsymbol{V}_L & -(\mathbb{T}_f^T)^+ \mathbb{T}_m^T \\ \mathbf{0}_{3p \times {}_pC_2} & \boldsymbol{E}_{3p} \end{bmatrix} \begin{bmatrix} \boldsymbol{f}^{int} \\ \boldsymbol{m}^{int} \end{bmatrix}. \tag{3.50}$$

Fig. 3.4 demonstrates the VL model applied to a humanoid robot in double stance ($p = 2$, Fig. 3.4A), double stance plus hand contact ($p = 3$, Fig. 3.4B), and double stance plus two-hand contact ($p = 4$, Fig. 3.4C).

The VL model is helpful in understanding the meaning of internal forces and moments. The model was introduced in humanoid robotics in [59]. There are some inherent problems, though, that hinder the implementation of the model. As already noted, the VL model is based on completely constrained contact joints; it cannot be directly adopted to account for frictionless contact joints. Frictionless contact joints are useful in such tasks as wiping a surface, for example. Clearly, the contact wrench components along the constrained motion directions contribute to the internal force/moments. Second, the VL model requires additional analysis to account for interdependent contact constraints. The contact constraints in the case of double stance, for example, are not independent. Referring to Fig. 3.4, it should be apparent that the two moments at the feet along the direction of the internal force are indeterminate: their sum contributes to the resultant moment at the loop-closure link, while their difference determines a component of the internal moment [59]. The dimension of $\mathcal{F}^{int}$ in (3.49) indicates seven internal force/moment components,[2] but in reality there are only six.

[2] Since $3p + {}_pC_2 = 6 + 1 = 7$.

Another problem with the VL model is that the parametrization of $\mathcal{R}(\boldsymbol{G}^T)$ via the internal force/moments, as in (3.49), is not straightforward.

### 3.5.3 Determining the Joint Torques in the Loop

The general solution to the WD problem, given in (3.39), is not plagued by the above-mentioned problems pertinent to the VL model. Indeed, the notation accounts for contact joints not only with, but also without friction. Note also that $\text{rank}\boldsymbol{N}\left(\mathbb{C}_{ce}(\boldsymbol{q}_e)\right)$ equals exactly the number of independent constraints in the closed loop. For example, for a double-stance posture with fully constrained feet contacts as above, $\text{rank}\boldsymbol{N}\left(\mathbb{C}_{ce}(\boldsymbol{q}_e)\right) = c_e - 6 = 12 - 6 = 6$. Furthermore, in the case of interdependent closed loops as those shown in Fig. 3.4B and C, there is a trivial but meaningful parametrization of the null-space contact wrench component, as will be shown in Section 3.6.2.

The net contact wrench components determined in (3.39) are realized with respective joint torques of the limbs constituting the closed loop. To clarify this, extract first the contact wrench components $\overline{\mathcal{F}}_k^c$ from the loop contact wrench (3.39) as follows:

$$\begin{aligned} \overline{\mathcal{F}}_k^c &= \mathbb{C}_{ck}^{\#}(\boldsymbol{q}_e)\mathcal{F}_e + \overline{\mathcal{F}}_k^n, \\ \overline{\mathcal{F}}_k^n &= \boldsymbol{N}_k\left(\mathbb{C}_{ce}(\boldsymbol{q}_e)\right)\overline{\mathcal{F}}_a^c(\boldsymbol{q}_e). \end{aligned} \tag{3.51}$$

Transforms $\mathbb{C}_{ck}^{\#}(\boldsymbol{q}_e) \in \Re^{c_k \times 6}$ and $\boldsymbol{N}_k(\mathbb{C}_{ce}(\boldsymbol{q}_e)) \in \Re^{c_k \times 12}$ are derived from the components of

$$\mathbb{C}_{ce}^{\#}(\boldsymbol{q}_e) \equiv \left[\begin{array}{c} \mathbb{C}_{ce_r}^{\#}(\boldsymbol{q}_e) \\ \hline \mathbb{C}_{ce_l}^{\#}(\boldsymbol{q}_e) \end{array}\right], \quad \boldsymbol{N}(\mathbb{C}_{ce}(\boldsymbol{q}_e)) \equiv \left[\begin{array}{c} \boldsymbol{N}_{e_r}(\mathbb{C}_{ce}(\boldsymbol{q}_e)) \\ \hline \boldsymbol{N}_{e_l}(\mathbb{C}_{ce}(\boldsymbol{q}_e)) \end{array}\right],$$

respectively. The two components of $\overline{\mathcal{F}}_k^c$ on the r.h.s. of (3.51) determine the respective joint torque components for the limb $k$, i.e.

$$\begin{aligned} \boldsymbol{\tau}_k^c &= \boldsymbol{\tau}_k^{ext} + \boldsymbol{\tau}_k^{int} \\ &= \boldsymbol{\mathcal{J}}_{cR}{}^T(\boldsymbol{q}_k)\mathbb{C}_{ck}^{\#}(\boldsymbol{q}_e)\mathcal{F}_e + \boldsymbol{\mathcal{J}}_{cR}{}^T(\boldsymbol{q}_k)\overline{\mathcal{F}}_k^n. \end{aligned} \tag{3.52}$$

The role of the first component is nominal compensation of the external wrench reaction $\mathcal{F}_e$. The second component can be used as internal wrench control input, to ensure that the reaction wrench $\mathcal{F}_k = \overline{\mathcal{F}}_k^c$ stays within $CWC_k$, and also as a force/moment control input. An illustrative example is presented in Section 3.6.5.

### 3.5.4 Which Generalized Inverse?

Determining the generalized inverse in the particular solution component in (3.39) is not a trivial problem. The Moore–Penrose pseudoinverse has been exploited in the field of multifinger grasping and multileg robots [43]. In analogy, the pseudoinverse was considered for double-stance balance of a humanoid robot [34,54]. It must be emphasized, though, that the use of the pseudoinverse for force distribution in humanoid robotics is inappropriate due to the following reasons. First, note that the dimensions of the reaction forces and moments

are nonuniform.[3] This problem can be eventually alleviated by resorting to an appropriate weighted generalized inverse [22,21,76]. Second, even if uniform dimensions can be assumed, there is another problem: the magnitudes of the components of the pseudoinverse (minimum-norm) solution are of the same order. This implies that the gravity force will always be approximately evenly distributed between the feet, irrespectively of the location of the CoM. This type of distribution is *inconsistent with statics*: the robot will not be able to lift its foot to make a step, for example, since the static equilibrium would be immediately lost. To accomplish such task, an *asymmetric* contact wrench distribution is needed, such that the contact wrench at the foot before lift-off becomes (almost) zero. This cannot be achieved with the pseudoinverse.

Furthermore, note that with the pseudoinverse, the loop-closure (or the loop-root) wrench is distributed evenly not only among the contacts, but also along the normal and the tangential directions at each contact joint with friction. It would be desirable, however, to distribute this wrench in a way that accounts for the Coulomb friction model. This is not possible since the model is based on inequalities. It is possible though to employ a weighted generalized inverse instead of the pseudoinverse, whereby the weights are determined to be in proportion to the friction coefficients $\mu_k$. With a weighted generalized inverse and without a null space component, the general solution (3.39) is rewritten as

$$\overline{\mathcal{F}}_e^c = \mathbb{C}_{ce}^{-W_\mu}(\boldsymbol{q}_e)\mathcal{F}_e. \tag{3.53}$$

The weight matrix is determined as $\boldsymbol{W}_\mu = \text{diag}\left[\boldsymbol{E}_{c_e^h} \quad \mu_{e_r}\boldsymbol{E}_{c_{e_r}^s} \quad \mu_{e_l}\boldsymbol{E}_{c_{e_l}^s}\right]$, under the convention pertinent to the contact joints with friction, i.e. $c_k = 6 = c_k^h + c_k^s$, $\eta_k = 0$ (cf. Section 3.3.2). With this approach, the decomposition of the external wrench $\mathcal{F}_e$ into normal and tangential components at the contacts satisfies the equality component in the contact FC model, so that the reaction force is exactly at the boundary of the friction cone. This approach can thus prevent sliding to occur at the contacts. On the other hand, the distribution of the normal reactions is as with the pseudoinverse since $\boldsymbol{E}_{c_e^h}$ determines equal weights for those reactions. In Section 5.10.4, another weighted generalized inverse will be introduced that can alleviate this problem.

### 3.5.5 Priorities Among the Joint Torque Components

Notation (3.52) introduces one more priority level into priority scheme (3.37), so now we have

$$\boldsymbol{\tau}_k^{ext} \succ \boldsymbol{\tau}_k^{int} \succ \boldsymbol{\tau}_k^m \succ \boldsymbol{\tau}_k^n. \tag{3.54}$$

Apparently, the self-motion joint torque for a kinematically redundant limb, $\boldsymbol{\tau}_k^n$, is at the lowest priority level; neither the reaction forces nor the forces in the unconstrained motion directions at the contact joints will be affected. The latter forces, on the other hand, do not affect

[3] In the field of multifinger hands and multileg robots the pseudoinverse solution is admissible since point contacts are assumed. In this case, the reactions are pure forces of uniform dimensions.

the internal force distribution and external force compensation. It is also seen that the internal force control, via $\boldsymbol{\tau}_k^{int}$, is possible without affecting the external force compensation. The external force affects all the other components; they may need readjustment after a change in $\mathcal{F}_R$. Note also that to satisfy the friction cone conditions, both $\boldsymbol{\tau}_k^{ext}$ and $\boldsymbol{\tau}_k^{int}$ should be controlled, as already clarified.

## 3.6 KINETOSTATIC RELATIONS OF A HUMANOID ROBOT

The independent closed-loop model discussed so far can be used for loop-specific controller design. Such a control approach might be appropriate for the purpose of analysis, e.g. to focus on pure balance control whereby the hands do not contact the environment, or on pure cooperative hand force control whereby the legs are fixed. In real applications, though, the force relations within the closed loops are always interdependent. Consider as an example the case depicted in Fig. 3.6. As already clarified, in this case there are two loop-closure links. The gravity force impressed on the object, $-\mathcal{G}_O$, directly acts within the closed loop of the arms. But this force is also structurally mapped at the base link, which is the root link of the other (the leg) closed loop. Consequently, $\mathcal{G}_O$ will contribute to the contact reactions at the feet, in addition to those at the hands. Another example is multicontact balance, whereby one of the hands or both are used to stabilize the posture of the robot. The respective model should account for the presence of a single loop-closure link (i.e. the static environment) and multiple interdependent branches.

In what follows, the independent closed-loop kinetostatic force relations derived in the previous sections will be modified to reflect such dependencies. The ultimate goal is to determine the joint torque components that:

1. compensate for gravity and other external wrenches acting at specified links (the base link and a hand-held object);
2. ensure an appropriate internal force in each closed loop to maintain the friction cone conditions or to obtain a desired end-link wrench to be used in force control;
3. determine the motion along the end-link mobility directions, in the case of frictionless contact joints;
4. ensure joint load redistribution, e.g. to minimize loads at specific joints.

The notation introduced in Section 2.11 for the instantaneous motion relations will be used thereby.

### 3.6.1 The Composite Rigid Body (CRB) and the CRB Wrench

The kinetostatic relations of a humanoid robot are derived under the assumption of locked joints. The robot behaves then as a composite rigid body (CRB), i.e. a system of interconnected links characterized by the net CoM and the inertia tensor [67]. In statics, the inertia tensor is irrelevant but the CoM plays an important role. A coordinate frame, denoted as $\{C\}$, is attached to the CoM. The coordinate axes are parallel to those of the base frame $\{B\}$. In what follows, the coordinate frame $\{C\}$ will be used in motion/force relations to represent the CRB.

As clarified in Section 3.4, the sum of all external wrenches acting on the robot links (i.e. the net external wrench) can be mapped at a characteristic link of interest, e.g. the base link, the CRB virtual "link" or the common loop-closure link.

Assume first that the net external wrench is mapped at the base link as $\mathcal{F}_B$. According to (3.25), $\mathcal{F}_B$ can be represented by the sum of appropriately mapped contact (reaction) wrenches $\mathcal{F}_k^c = \mathcal{F}_k,\ k \in \{e_r, e_l\},\ e \in \{F,\ H\}$.[4] In the general case, i.e. when some of the contact joints are frictionless, $\mathcal{F}_B$ can be expressed according to (3.38) as the sum of reaction wrench components along the constrained motion directions, $\overline{\mathcal{F}}_k^c$, mapped by the contact map of the robot, i.e.

$$\mathcal{F}_B = \sum_k \mathbb{C}_{cB}(\boldsymbol{q}_k)\overline{\mathcal{F}}_k^c = \mathbb{C}_{cB}(\boldsymbol{q})\overline{\mathcal{F}}^c. \tag{3.55}$$

Here $\overline{\mathcal{F}}^c \in \Re^c$ is composed of the stacked $\overline{\mathcal{F}}_k^c$ contact wrenches, ordered according to the $k, e$ subscript convention. The mapping of the net external wrench at the CRB frame can be written in a similar form, i.e.

$$\mathcal{F}_C = \sum_k \mathbb{C}_{cC}(\boldsymbol{q}_k)\overline{\mathcal{F}}_k^c = \mathbb{C}_{cC}(\boldsymbol{q})\overline{\mathcal{F}}^c. \tag{3.56}$$

As an example, consider a double-stance posture ($k \in \{F_r,\ F_l\}$) with frictional constraints. Such posture appears quite often in practice; $\mathcal{F}_{(\circ)}$ can then be written as

$$\mathcal{F}_{(\circ)} = \begin{bmatrix} \boldsymbol{f}_{(\circ)} \\ \boldsymbol{n}_{(\circ)} \end{bmatrix} = \sum_k \begin{bmatrix} \boldsymbol{E}_3 & \boldsymbol{0}_3 \\ -[\boldsymbol{r}^{\times}_{\overleftarrow{(\circ)k}}] & \boldsymbol{E}_3 \end{bmatrix} \begin{bmatrix} \boldsymbol{f}_k \\ \boldsymbol{m}_k \end{bmatrix}, \tag{3.57}$$

subscript $_{(\circ)}$ standing for either $_B$ or $_C$. $\boldsymbol{f}_k$ and $\boldsymbol{m}_k$ denote the ground reaction force (GRF) and the ground reaction moment (GRM) at the foot. They constitute the foot contact (reaction) wrench $\mathcal{F}_k^c$. Note that when the GRF-induced GRM is subtracted from the CRB wrench, one obtains the following net wrench:

$$\mathcal{F}_{net} \equiv \mathcal{F}_{(\circ)} - \sum_k \begin{bmatrix} \boldsymbol{0}_3 \\ [\boldsymbol{r}^{\times}_{\overleftarrow{(\circ)k}}]\boldsymbol{f}_k \end{bmatrix}, \tag{3.58}$$

s.t.

$$\mathcal{F}_{net} = \sum_k \mathcal{F}_k^c.$$

The net wrench $\mathcal{F}_{net}$ will be used in Section 5.10.4. Furthermore, note that the above relations can be reformulated for the case when the net external wrench is mapped at the common loop-closure link, i.e. the floor coordinate frame $\{F\}$. This is done straightforwardly by replacing the $_{(\circ)}$ subscripts with $_F$. A notation involving $\mathcal{F}_F$ will appear in Section 7.8.3. The net

[4] For clarity and without loss of generality, henceforth it is assumed that contact joints are established at the end links. In general, a contact joint can be established at anybody segment.

wrench acting on the CRB will be henceforth referred to as the *CRB wrench*, or simply as the *body wrench*.

The action of the gravity field on the CRB can be expressed either by a distributed model of gravity wrenches acting on each robot link, or by a lumped model, s.t. the net gravity *force* acts at the system CoM. These two representations are related to the two notations in the base and the mixed quasicoordinates, respectively. Consider first the distributed model. The reaction to the gravity wrench acting on the base link is written as

$$\mathcal{G}_B \equiv \begin{bmatrix} \boldsymbol{g}_f \\ \boldsymbol{g}_m \end{bmatrix} = M \begin{bmatrix} -\boldsymbol{E}_3 \\ [\boldsymbol{r}^{\times}_{\overleftarrow{BC}}] \end{bmatrix} \boldsymbol{a}_g. \tag{3.59}$$

Here $\boldsymbol{r}_{\overleftarrow{BC}}$ is the position of the base-link frame w.r.t. the CoM, $\boldsymbol{a}_g = \begin{bmatrix} 0 & 0 & -g \end{bmatrix}^T$, and $g$ and $M$ stand for the acceleration of the gravity and the total mass, respectively. The gravity wrenches acting on the rest of the links are compensated by the following gravity *joint torque*:

$$\boldsymbol{g}_\theta = M \boldsymbol{J}^T_{\overleftarrow{BC}} \boldsymbol{a}_g = -\boldsymbol{J}^T_{\overleftarrow{BC}} \boldsymbol{g}_f, \tag{3.60}$$

where $\boldsymbol{J}_{\overleftarrow{BC}}$ denotes the net-CoM Jacobian (cf. (2.117)).

The lumped-model representation yields a simpler relation. The reaction to the gravity wrench acting on the CRB is $\mathcal{G}_C \equiv \begin{bmatrix} \boldsymbol{g}_f^T & \boldsymbol{0}^T \end{bmatrix}^T$, i.e. there is no moment component, as expected.

### 3.6.2 Interdependent Closed Loops

The above notation refers to humanoid robot postures forming interdependent closed loops, in the general case of mixed friction/frictionless contact joints. For example, when the contact joints at the feet are with friction and those at the hands are frictionless, then

$$\overline{\mathcal{F}}^c = \begin{bmatrix} (\mathcal{F}^c_{F_r})^T & (\mathcal{F}^c_{F_l})^T & (\overline{\mathcal{F}}^c_{H_r})^T & (\overline{\mathcal{F}}^c_{H_l})^T \end{bmatrix}^T, \tag{3.61}$$

$\mathcal{F}^c_{F_j} = \mathcal{F}_{F_j}$ denoting the friction wrenches at the feet. When all contact joints are with friction ($c = 24$), then $\overline{\mathcal{F}}^c = \mathcal{F}^c = \mathcal{F} \in CWC$ and

$$CWC = CWC_{F_r} \times CWC_{F_l} \times CWC_{H_r} \times CWC_{H_r} \subset \Re^{24}.$$

In the case of multicontacts, e.g. double stance or double stance plus hand contact(s), as in Fig. 3.4, the base link will be unilaterally overconstrained since $c > 6$. Given the CRB wrench $\mathcal{F}_B$, there is an infinite set of contact wrenches (cf. (3.39)), i.e.

$$\overline{\mathcal{F}}^c = \overline{\mathcal{F}}^{ext} + \overline{\mathcal{F}}^n, \tag{3.62}$$

$$\overline{\mathcal{F}}^{ext} = \mathbb{C}^{\#}_{cB}(\boldsymbol{q}) \mathcal{F}_B,$$

$$\overline{\mathcal{F}}^n = \boldsymbol{N}(\mathbb{C}_{cB}(\boldsymbol{q})) \overline{\mathcal{F}}^c_a. \tag{3.63}$$

The second term on the r.h.s. is a component from the null space $\mathcal{N}(\mathbb{C}_{cB})$, parametrized by an arbitrary composite contact wrench, $\overline{\mathcal{F}}_a^c \in \Re^c$. Recall that the number of internal force/moments within the closed loops equals the rank of the null-space projector, which is $c-6$. This is also apparent from the dimension of $\overline{\mathcal{F}}^{int}(\boldsymbol{q}_e)$ in (3.41), which is a minimal-parametrization vector. However, as noted at the end of Section 3.5.2, how to specify the internal force/moments is not always intuitively clear. The nonminimal parametrization, on the other hand, can be specified in a straightforward way since the meaning is that of a contact wrench. Indeed, note that a number of practical tasks require precise contact wrench control at the hands. In this case, with the nonminimal parametrization it is possible to specify the reference hand contact wrenches *directly* as null-space contact wrench components. To this end, (3.62) is partitioned first as

$$\begin{bmatrix} \overline{\mathcal{F}}_F^c \\ \overline{\mathcal{F}}_H^c \end{bmatrix} = \begin{bmatrix} \left(\mathbb{C}_{cB}^{\#}\right)_F \\ \left(\mathbb{C}_{cB}^{\#}\right)_H \end{bmatrix} \mathcal{F}_B + \begin{bmatrix} \boldsymbol{N}_F(\mathbb{C}_{cB}) \\ \boldsymbol{N}_H(\mathbb{C}_{cB}) \end{bmatrix} \overline{\mathcal{F}}_a^c, \tag{3.64}$$

the upper and lower blocks standing for contact wrench components for the feet and hands, respectively. Furthermore, it is assumed that the reference hand contact wrench $(\overline{\mathcal{F}}_H^c)^{ref}$ is obtained from a conventional force/moment controller. Then, the lower equation can be employed to obtain the parametrization vector as

$$\overline{\mathcal{F}}_a^c = \boldsymbol{N}_H^+(\mathbb{C}_{cB}) \left( (\overline{\mathcal{F}}_H^c)^{ref} - \left(\mathbb{C}_{cB}^{\#}\right)_H \mathcal{F}_B \right). \tag{3.65}$$

With this parametrization, the WD problem is solved as

$$\begin{bmatrix} \overline{\mathcal{F}}_F^c \\ \overline{\mathcal{F}}_H^c \end{bmatrix} = \begin{bmatrix} \left(\mathbb{C}_{cB}^{\#}\right)_F \mathcal{F}_B + \boldsymbol{N}_F(\mathbb{C}_{cB}) \boldsymbol{N}_H^+(\mathbb{C}_{cB}) \left( \overline{\mathcal{F}}_H^{ref} - \left(\mathbb{C}_{cB}^{\#}\right)_H \mathcal{F}_B \right) \\ (\overline{\mathcal{F}}_H^c)^{ref} \end{bmatrix}. \tag{3.66}$$

Hereby, $\boldsymbol{N}_H \boldsymbol{N}_H^+ = \boldsymbol{E}$ was used. Apparently, the reference hand contact wrenches appear *directly* as contact wrenches at the hands. The distribution of the CRB wrench at the feet depends on the type of generalized inverse (cf. Section 3.5.4), as well as on the reference hand contact wrenches.

### 3.6.3 Independent Closed Loops

In the case of two independent closed loops, i.e. as in the example in Fig. 3.6, the internal force/moments within each closed loop are noninterfering. Assume that the total external wrench at the base link is $-\mathcal{F}_B$. According to (3.25), this wrench is determined by the external wrenches acting at the links, e.g. the gravity wrenches at the base and the hand-held object, s.t. $-\mathcal{F}_B = -\mathcal{G}_B - \mathbb{T}_{\underleftarrow{BO}}^T \mathcal{G}_O$. Other external wrenches, e.g. resulting from a sudden push on an arbitrary link, could be added in a straightforward way. To account for the independent closed loops, rewrite (3.55) as

$$\mathcal{F}_B = \sum_k \mathbb{C}_{cB}(\boldsymbol{q}_k) \overline{\mathcal{F}}_k^c = \mathbb{C}_{cB}(\boldsymbol{q}_F) \overline{\mathcal{F}}_F^c + \mathbb{C}_{cB}(\boldsymbol{q}_H) \overline{\mathcal{F}}_H^c. \tag{3.67}$$

The term $\overline{\mathcal{F}}_e^c \in \Re^{c_e}$ is composed by stacking the two $\overline{\mathcal{F}}_{k=e_j}^c$ components. Further on, the external wrench acting on the loop-closure link (i.e. the hand-held object) is $-\mathcal{F}_H = -\mathcal{G}_O$. This wrench is represented as the following sum (cf. (3.30)):

$$\mathcal{F}_H = \sum_j \mathbb{C}_{cH_j}(\boldsymbol{q}_{H_j})\overline{\mathcal{F}}_{H_j}^c = \mathbb{C}_{cH}(\boldsymbol{q}_H)\overline{\mathcal{F}}_H^c. \tag{3.68}$$

Hand reaction wrenches can be obtained from this relation in an infinite number of ways. We have

$$\overline{\mathcal{F}}_H^c = \mathbb{C}_{cH}^{\#}(\boldsymbol{q}_H)\mathcal{F}_H + \boldsymbol{V}\big(\mathbb{C}_{cH}(\boldsymbol{q}_H)\big)\overline{\mathcal{F}}_H^{int}. \tag{3.69}$$

Note that the second term on the r.h.s. determines the hand reaction wrenches from the null space $\mathcal{N}\left(\mathbb{C}_{cH}(\boldsymbol{q}_H)\right)$ via the internal force/moments $\overline{\mathcal{F}}_H^{int} \in \Re^{c_H-6}$. Recall that $\boldsymbol{V}$ denotes the minimal representation of the null-space basis vectors. Then, substitute (3.69) into (3.67) and solve for the contact wrenches at the feet, i.e.

$$\begin{aligned}\overline{\mathcal{F}}_F^c &= \mathbb{C}_{cB}^{\#}(\boldsymbol{q}_F)\left(\mathcal{F}_B - \mathcal{F}_{B_H}\right) + \boldsymbol{V}\big(\mathbb{C}_{cB}(\boldsymbol{q}_F)\big)\overline{\mathcal{F}}_F^{int},\\ \mathcal{F}_{B_H} &\equiv \mathbb{C}_{cB}(\boldsymbol{q}_H)\left(\mathbb{C}_{cH}^{\#}(\boldsymbol{q}_H)\mathcal{F}_H + \boldsymbol{V}\big(\mathbb{C}_{cH}(\boldsymbol{q}_H)\big)\overline{\mathcal{F}}_H^{int}\right).\end{aligned} \tag{3.70}$$

The net contact and internal wrenches are then assembled by stacking the respective components, i.e.

$$\begin{aligned}\overline{\mathcal{F}}^c &= \left[(\overline{\mathcal{F}}_F^c)^T \quad (\overline{\mathcal{F}}_H^c)^T\right]^T \in \Re^c,\\ \overline{\mathcal{F}}^{int} &= \left[(\overline{\mathcal{F}}_F^{int})^T \quad (\overline{\mathcal{F}}_H^{int})^T\right]^T \in \Re^{c-6}.\end{aligned}$$

### 3.6.4 Determining the Joint Torques

To determine the joint torque components, first derive the individual reaction wrench components, $\overline{\mathcal{F}}_k^c = \overline{\mathcal{F}}_k^{\,ext} + \overline{\mathcal{F}}_k^{\,n}$, from the total reaction wrench. This is done in a straightforward way by making use of (3.51). The internal force component, $\overline{\mathcal{F}}_k^{\,n} = \boldsymbol{N}_k\big(\mathbb{C}_{cR}(\boldsymbol{q})\big)\overline{\mathcal{F}}_a^c$, can then be used as a control input to ensure that the reaction wrench stays within the $CWC_k$ at all times. This component can also be used in end-link force control. The limb joint torque components $\boldsymbol{\tau}_k^{\,ext}$ and $\boldsymbol{\tau}_k^{\,int}$ can then be calculated. These components are consequently summed up with components due to the motion in the mobility directions and the kinematic redundancy, $\boldsymbol{\tau}_k^{\,m}$ and $\boldsymbol{\tau}_k^{\,n}$, to obtain the limb joint torque $\boldsymbol{\tau}_k$. The joint torques of all limbs are stacked as follows:

$$\boldsymbol{\tau} = \begin{bmatrix}\boldsymbol{\tau}_{F_r}^T & \boldsymbol{\tau}_{F_l}^T & \boldsymbol{\tau}_{H_r}^T & \boldsymbol{\tau}_{H_l}^T\end{bmatrix}^T \in \Re^n. \tag{3.71}$$

Note also that, similarly to (3.33),

$$\boldsymbol{\tau} = \begin{bmatrix}\mathcal{J}_{cB}^T(\boldsymbol{q}) & \mathcal{J}_{mB}^T(\boldsymbol{q})\end{bmatrix}\begin{bmatrix}\overline{\mathcal{F}}^c\\ \overline{\mathcal{F}}^m\end{bmatrix} = \boldsymbol{\tau}^{\,c} + \boldsymbol{\tau}^{\,m}. \tag{3.72}$$

Here $\overline{\mathcal{F}}^m \in \Re^\eta$ is composed of $\overline{\mathcal{F}}_k^m$ vectors stacked in the same order as the components of $\overline{\mathcal{F}}^c$. Further on, when kinematic redundancy is present, a null space component from $\mathcal{N}^*\big(\boldsymbol{J}_R(\boldsymbol{q})\big)$ can be added. As a result, the joint torque of the humanoid robot is expressed as the sum

$$\boldsymbol{\tau} = \boldsymbol{\tau}^{ext} + \boldsymbol{\tau}^{int} + \boldsymbol{\tau}^m + \boldsymbol{\tau}^n. \tag{3.73}$$

The components are arranged in the following priority scheme (cf. (3.54)):

$$\boldsymbol{\tau}^{ext} \succ \boldsymbol{\tau}^{int} \succ \boldsymbol{\tau}^m \succ \boldsymbol{\tau}^n.$$

Component $\boldsymbol{\tau}^n$ appears whenever there is kinematic redundancy. Component $\boldsymbol{\tau}^m$ is available when there are frictionless contact joints or completely unconstrained end links. The internal wrench component $\boldsymbol{\tau}^{int}$ stems from redundant actuation within a closed kinematic loop. Component $\boldsymbol{\tau}^{ext}$ is always present.

The joint torque that ensures the static balance can be expressed, either with the distributed or the lumped CRB model, as

$$\boldsymbol{\tau}_B = \boldsymbol{g}_\theta - \boldsymbol{\mathcal{J}}_{cR}^T \overline{\mathcal{F}}^c(\mathcal{G}_B), \tag{3.74}$$

$$\boldsymbol{\tau}_M = -\boldsymbol{\mathcal{J}}_{cM}^T \overline{\mathcal{F}}^c(\mathcal{G}_C), \tag{3.75}$$

respectively. Using the expression for the Jacobian $\boldsymbol{\mathcal{J}}_{cM}$ given in (2.126), it is straightforward to prove that $\boldsymbol{\tau}_B = \boldsymbol{\tau}_M$. This is the reason why the gravity joint torque $\boldsymbol{g}_\theta$ does not explicitly appear in the last equation. An important remark is due at this point with regard to the usage of the above expressions in a controller. In the case of balance control, for example, quite often a reference contact wrench $(\overline{\mathcal{F}}^c)^{ref}$ is employed. In this case, the above two equations are not equivalent. Note that the gravity torque $\boldsymbol{g}_\theta$ in (3.74) can be used as an exact gravity compensation term. On the other hand, $\boldsymbol{\tau}_M$ does not provide for exact gravity compensation since the gravity joint torque becomes a function of $(\overline{\mathcal{F}}^c)^{ref}$.

### 3.6.5 Illustrative Examples

#### *Double Stance on Flat Floor in 2D (Lateral Plane)*

A lower-body biped model on the plane with four joints is shown in Fig. 3.5. It is assumed that the feet are fully constrained, s.t. $c_{F_j} = 3$. Thus, the contact wrenches $\mathcal{F}_{F_j}^c$ comprise one GRM and two GRF components. The static-balance condition for the closed loop is $\mathcal{G}_B = \mathbb{C}_{cB}(\boldsymbol{q}_F)\,\mathcal{F}^c(\boldsymbol{q}_F)$. The general solution to the WD problem (cf. (3.39)) can be written as

$$\begin{aligned}\mathcal{F}^c(\boldsymbol{q}_F) &= \mathbb{C}_{cB}^{\#}(\boldsymbol{q}_F)\,\mathcal{G}_B + \boldsymbol{N}\left(\mathbb{C}_{cB}(\boldsymbol{q}_F)\right)\mathcal{F}_a^c(\boldsymbol{q}_F)\\ &= \mathbb{C}_{cB}^{\#}(\boldsymbol{q}_F)\,\mathcal{G}_B + \boldsymbol{V}\left(\mathbb{C}_{cB}(\boldsymbol{q}_F)\right)\overline{\mathcal{F}}^{int}(\boldsymbol{q}_F).\end{aligned}$$

With the help of the VL model, this solution can be rewritten as

$$\mathcal{F}^c(\boldsymbol{q}_F) = \mathbb{C}_{cB}^{+}(\boldsymbol{q}_F)\,\mathcal{G}_B + \boldsymbol{V}_L\, f_{rl}^{int},$$

where

$$\boldsymbol{V}_L = \begin{bmatrix}\boldsymbol{e}_{rl}^T & \boldsymbol{e}_{lr}^T\end{bmatrix}^T = \begin{bmatrix}0 & 1 & 0 & 0 & -1 & 0\end{bmatrix}^T.$$

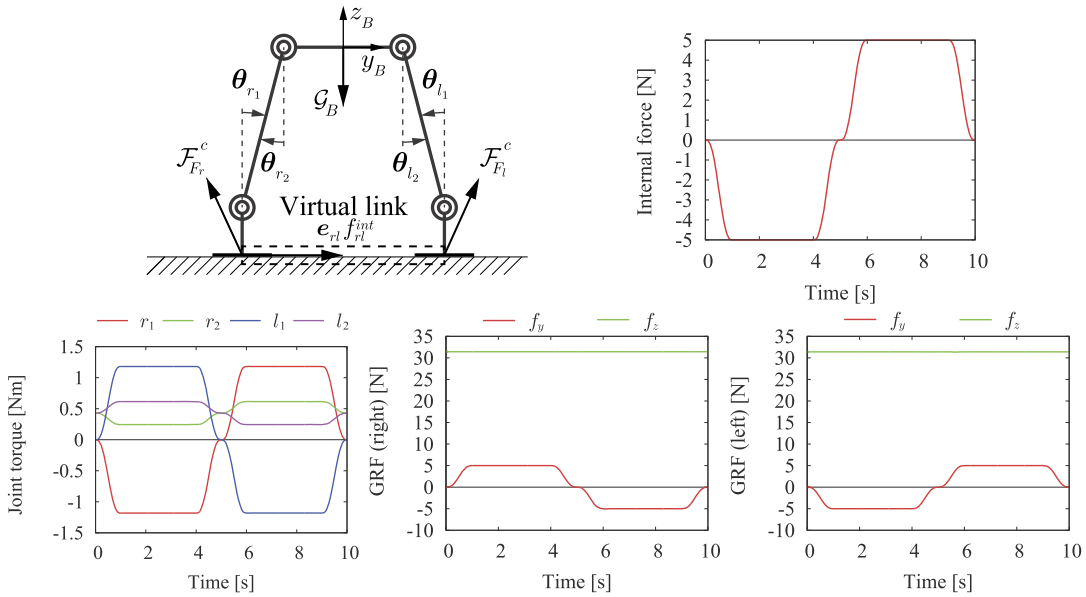


**FIGURE 3.5** Double stance with a five-link biped on the plane. The magnitude of the internal force, $f^{int}_{rl}$, is shown in the upper-right figure. The internal force is changed smoothly, initially with compression (negative), then with extension (positive). The respective joint torque and GRF variations are shown in the lower row. The GRMs equal the ankle torques, denoted as $r_1$ and $l_1$ in the lower-left figure.

Three remarks are due. First, the number of the internal force/moment components is three: the internal force $f^{int}_{rl}$ and the two GRMs $m_{F_j}$. Second, note that the internal moments are not considered in the above equation. Third, the pseudoinverse was adopted as a generalized inverse in the solution. With this choice, the vertical GRFs are distributed equally. No problem arises in this particular example with such distribution. This is not the case, however, in general, as already discussed. An example that highlights the problem stemming from the pseudoinverse-based WD will be introduced shortly.

The joint torque vector can be derived as

$$\begin{aligned}
\boldsymbol{\tau} &= \boldsymbol{g}_\theta - (\boldsymbol{\tau}^{ext} + \boldsymbol{\tau}^{int}), \\
\boldsymbol{\tau}^{ext} &= \mathcal{J}^T_{cR}(\boldsymbol{q}_F)\, \mathbb{C}^+_{cB}(\boldsymbol{q}_F)\, \mathcal{G}_B, \\
\boldsymbol{\tau}^{int} &= \mathcal{J}^T_{cR}(\boldsymbol{q}_F) \boldsymbol{V}_L f^{int}_{rl}.
\end{aligned}$$

The balance of force/moments in the closed loop is examined by varying the internal force within a symmetric posture, the ankle/hip joints being set at $5/-5$ degrees, respectively. The magnitude of the internal force is changed between $\pm 5$ N smoothly, with the help of fifth-order splines. The respective variations of all force/moment and joint torque components are shown in the lower row of Fig. 3.5. The model parameters were derived from those of a miniature humanoid robot HOAP-2 (cf. Chapter A). Note that the ankle torques (the GRMs)

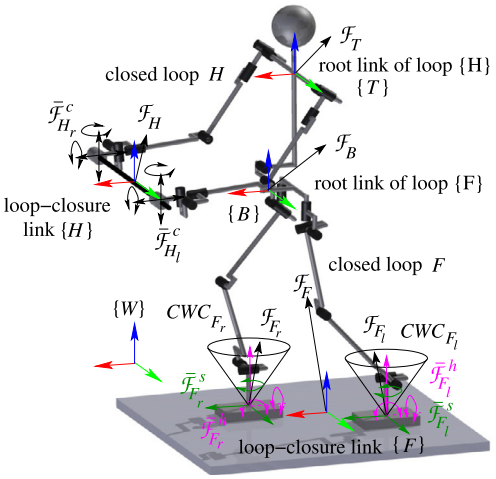


**FIGURE 3.6** A humanoid robot with two independent closed loops, $F$ and $H$, formed with contact joints at the feet (with friction) and hands (frictionless). The reaction wrenches acting at the loop-closure and loop-root links are denoted as $\mathcal{F}_e,\ e \in \{F, H\}$, and $\mathcal{F}_R,\ R \in \{B, T\}$, respectively. The reaction wrench components along the constrained and unconstrained motion directions at the hands are denoted as $\overline{\mathcal{F}}^c_{H_j},\ j \in \{r, l\}$, and $\overline{\mathcal{F}}^m_{H_j}$, respectively (the latter are not shown). The reaction wrench components along the hard- and soft-constraint directions at the feet stem from friction. They are denoted as $\overline{\mathcal{F}}^h_{F_j}$ and $\overline{\mathcal{F}}^s_{F_j}$, respectively. The total friction/contact wrench $\mathcal{F}_{F_j}$ is confined within the contact wrench cone $CWC_{F_j}$.

determine the internal moment in the chain. Apparently, they are sufficiently small, s.t. the net CoP (not shown) stays well within the interior of the BoS. Therefore, no foot roll is observed.

### *Double Stance on Flat Floor With Friction*

Next, consider the example shown in Fig. 3.6 of a humanoid robot in 3D on flat ground. The contact joints at the hands are assumed frictionless while those at the feet are with friction. The friction model is the polyhedral CWC (four-sided pyramid) one. Motion at the feet is then completely constrained, s.t. $c_{F_j} = 6,\ \eta_{F_j} = 0$. The motion constraints stem from the normal reactions $\overline{\mathcal{F}}^h_k \in \Re^{c^h_k}$ and the reactions to the tangential friction forces, $\overline{\mathcal{F}}^s_k \in \Re^{c^s_k}$. These reactions sum up as in (3.29), whereby contact wrenches $\mathcal{F}_{F_j} = \mathcal{F}^c_{F_j} \in CWC_{F_j}$. The feet do not slip therefore. It should be noted that the contact wrenches can be estimated (e.g. according to the algorithms explained in Chapter 4) and/or obtained from the sensors attached at the end links. The sensors could be either multiaxis force/torque sensors or arrays of single-axis pressure sensors, such as force sensing resistors (FSRs). Details about such sensors can be found in Section 3.2 of [36].

Further on, note that since the feet contacts are with friction, the base will be *unilaterally overconstrained*, i.e. $\mathcal{F}_B = \mathbb{T}^T_{\underleftarrow{BF_r}}(\boldsymbol{q}_{F_r})\mathcal{F}_{F_r} + \mathbb{T}^T_{\underleftarrow{BF_l}}(\boldsymbol{q}_{F_l})\mathcal{F}_{F_l}$. This also implies that the gravity wrench impressed on the base link can be compensated by the net reaction wrench at the base, so $\mathcal{F}_B = -\mathcal{G}_B = -(\mathcal{G}^h_B + \mathcal{G}^s_B)$.

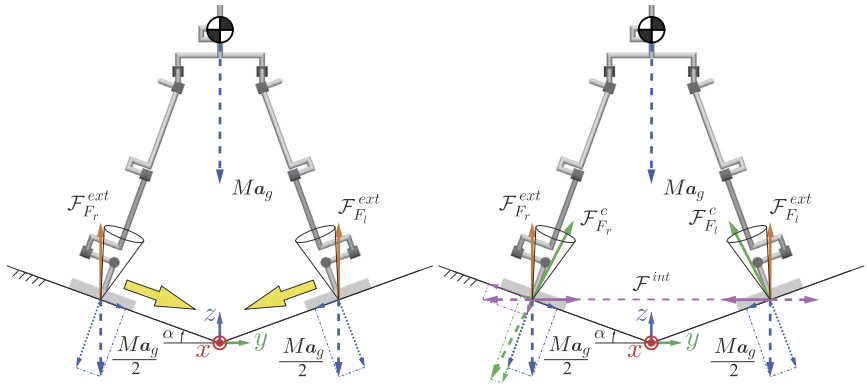


**FIGURE 3.7** When supported on inclined surfaces, the force of gravity induces total reactions $\mathcal{F}_{F_j}^{ext}$ comprising components in the normal and tangential directions at each contact. Left (A): Zero internal force case. The tangential reaction components lead to slipping because of insufficient surface friction. Right (B): Nonzero internal force case. The slipping can be avoided with the help of a properly defined internal force or a weighted generalized inverse that modifies the magnitudes of the normal and tangential reaction components, s.t. the total reaction $\mathcal{F}_{F_j}^{c}$ is within the CWC.

### *Double Stance on Frictionless Flat Floor*

Next, consider the case of frictionless contact joints at the feet. The net reaction wrench at the base then becomes $\mathcal{F}_B = \mathcal{F}_B^c = \mathbb{C}_{cR}(\boldsymbol{q}_{F_r})\overline{\mathcal{F}}_{F_r}^c + \mathbb{C}_{cR}(\boldsymbol{q}_{F_l})\overline{\mathcal{F}}_{F_l}^c$. Note that the quasistatic body wrench component $\mathcal{F}_B^m = -\mathcal{G}_B^m$ does not appear in the above relation.

### *Double Stance With Noncoplanar Contacts*

The role of the component $-\mathcal{G}_B^m$ becomes apparent when the feet are placed on inclined support surfaces with relatively low friction, as in Fig. 3.7. This example demonstrates the case of an *underconstrained* base and thus of an uncontrollable robot. Since the feet are in contact with inclined surfaces, the gravity force generates components in both the normal and the tangential directions at the contact joints. Low friction implies that the reactions will be outside the CWC, as shown in Fig. 3.7A. The reactions in the tangential directions will then induce foot acceleration and the robot will become uncontrollable. This problem can be solved by applying appropriate joint torques that work against the reactions in the tangential directions, s.t. the CWC conditions will be satisfied. These joint torque components are computed from the internal force. In other words, $\boldsymbol{\tau}_{F_r}^{int}$ and $\boldsymbol{\tau}_{F_l}^{int}$ can be used to ensure the static equilibrium at the selected posture, despite the presence of a low friction (cf. Fig. 3.7B). This is evident from the simulation results shown in Fig. 3.8 and Video 3.6-1 [33]. In the simulation, a small-size robot with parameters similar to those of a HOAP-2 robot [25] was used (see Section A.1). Initially, a nonzero internal force is applied to ensure the static equilibrium. At $t = 1$ s, the internal force is gradually decreased which results in foot sliding (apparent from the foot position graphs). After keeping the internal force at zero for a while, it is then increased gradually to stop the sliding. It should be mentioned that this behavior cannot be achieved with pure static control because of the motion during the sliding phase. Notice that the robot is uncontrollable during this phase. This is why large errors appear when stopping

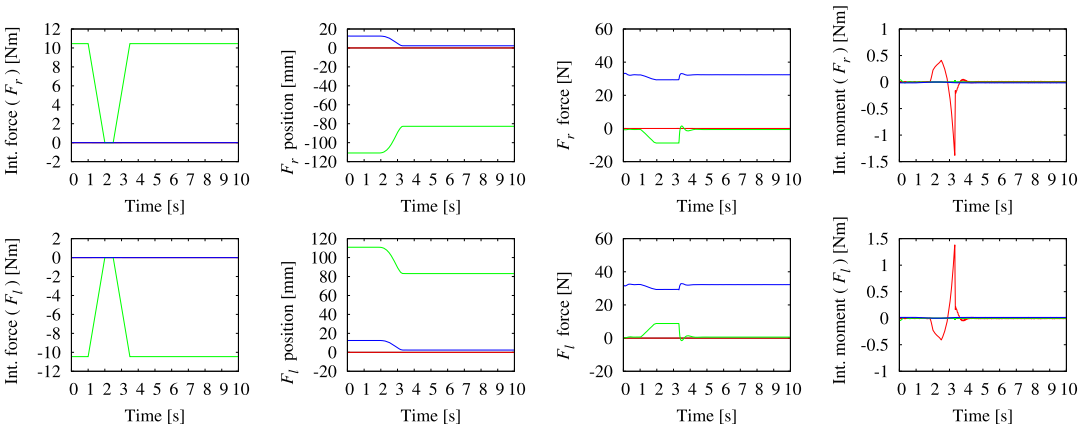


**FIGURE 3.8** Simulation results of double stance on inclined surfaces (cf. Fig. 3.7). Right/left foot data are shown in the upper/lower rows, respectively. The RGB color convention is used for the $xyz$-components. The internal force is first used to initialize foot sliding, then to stop it. Details about the controller can be found in Section 5.10.4.

is initialized. These errors result in relatively large internal moments that need to be controlled to ensure that the feet CoPs stay within the interiors of the footprints. Further details about the controller used in this simulation can be found in Section 5.10.4.

***Double Stance on Flat Floor With High/Zero Friction at the Right/Left Foot***

Finally, for the sake of completeness, consider also the general case of contact joints with and without friction. For example, let the right foot be constrained with sufficient friction, while the left foot is placed on a frictionless surface. The net reaction wrench at the base link is $\mathcal{F}_B = \mathbb{T}^T_{\overleftarrow{BF_r}}(\boldsymbol{q}_{F_r})\,\mathcal{F}_{F_r} + \mathbb{C}_{cB}(\boldsymbol{q}_{F_l})\,\overline{\mathcal{F}}^c_{F_l}$. The base link is *unilaterally fully constrained* by the unilateral contact at the right foot. Note, however, that the wrench component from the left foot may introduce an additional independent constraint. Thus, the base link may become (conditionally) overconstrained.

## 3.6.6 Summary and Discussion

The kinetostatic relations in closed-loop chains are determined by the total external wrench acting at the loop and the (internal) joint torques of the limbs constituting the closed loop. The total external wrench is the sum of all external wrenches applied at one or more links within the loop, mapped at a link of preference, e.g. the base link. The mapping is structural, i.e. it depends on the configuration of the loop. The action of the joint torques, on the other hand, results in a wrench mapped via inverses of the transposed limb Jacobians at the base link. This wrench is in balance with the total external wrench.

Further on, the action of the external wrenches and the joint torques induces wrenches at the contact joints, called reaction wrenches. These wrenches should be controlled in appropriate ways to ensure the satisfaction of the friction cone conditions at the contact joints while compensating the action of the external wrenches. The joint torque of the limb that

ensures a desired reaction wrench at the respective contact joint can be obtained in a straightforward manner. The internal force within the closed loop gives rise to another joint torque component to meet the friction cone conditions. The role of the internal force is to modify the contact wrenches without changing the force balance at the base link. For example, the maximum contact wrench along the unconstrained motion directions can be minimized via the internal force to avoid the initialization of slipping. This task can be performed independently from the postural balance task, which depends on the force balance at the base link. These relations play important roles in posture stability and torque optimization, as will be shown in the following section.

In motion/force control tasks, such as surface cleaning, it might be more appropriate to involve frictionless-contact joint models. Such models are also used in the case of completely unconstrained motion of the end links, e.g. of the hands and the foot of the swing leg during walking. The motion along the unconstrained (mobility) directions is determined by *task-based* constraints rather than by physical ones. When frictionless-joint models become involved, the relations derived in this section are better characterized as quasistatic rather than purely static. In fact, the motion along the mobility directions is determined by dynamic forces. This issue will be discussed in Chapter 4. Another example of a kinetostatic relation stems from a redundant actuation that is inherent to kinematically redundant limbs. A redundantly actuated limb can be subjected to an infinite number of joint torques that do not alter the contact wrench. An appropriate torque can then be selected, e.g. to minimize the load of a given actuator.

The static/kinetostatic force relations derived in this section are of a general nature. The results can be used in the case of varying contact conditions and topology changes, e.g. as a result of establishing/breaking contacts.

## 3.7 STATIC POSTURE STABILITY AND OPTIMIZATION

Static posture stability plays an important role in a motion generation approach based on a sequence of static postures [29,30,6,7,23]. A posture is said to be stable in the static sense when, given a static initial condition, the total external wrench acting on the CRB (e.g. the wrench of gravity plus the reaction wrenches) does not induce any motion. A statically stable posture is characterized with *robustness* [52,14]. Robustness implies that the stability of the posture will be ensured not only for the acting external wrench, but also for the nearby wrenches. Optimization of a static posture refers to the process of increasing its robustness, which can be achieved via the internal joint torque component. As already clarified, this torque component is related to friction. In the presence of high friction, for example, the optimization objective can be set as a minimization of the maximum component of the (reaction) contact wrench $\overline{\mathcal{F}}^c$. On the other hand, when the friction is not as high and there is a possibility of slip, the optimization is based on the objectives of an appropriate CRB posture and internal WD. As a result, the reaction wrenches can be eventually confined within the interior of the CWC. Referring to (3.62), a minimax optimization in the high-friction case can be achieved by employing the pseudoinverse in the particular solution. Such a solution is inappropriate, however, in the lower-friction case. The output of the optimization process

yields the joint torque components $\boldsymbol{\tau}^{ext}$ and $\boldsymbol{\tau}^{int}$ (cf. (3.73)). Furthermore, the joint torque limits should also be taken in consideration during the optimization process, via the force component $\boldsymbol{\tau}^{n}$, when kinematic redundancy is present.

### 3.7.1 Static Posture Stability

In the field of multifinger grasping, the stability of a grasp has been related to the so-called *force closure* [49,10] (cf. Chapter 6). A force-closure grasp is defined by a set of reaction forces $\overline{\mathcal{F}}^{c} \in CWC$ such that $\mathbb{G}\,\overline{\mathcal{F}}^{c} = \mathcal{F}_O$, where $\mathcal{F}_O$ denotes the reaction to an external spatial force applied at the grasped object and $\mathbb{G}$ is the grasp map, which is an equivalent of the contact map $\mathbb{C}_{cR}$ (or $\mathbb{C}_{cC}$) introduced here. With a force-closure grasp, the instability problem due to the unilateral motion constraints at the fingertips can be effectively solved. From the viewpoint of a humanoid robot, force-closure grasps can be characterized as "strongly stable" since the grasp map and friction conditions admit *any* external force.

Humanoid robots, though, cannot attain force closure–like postures because of their human-like design. Therefore, the instability problem stemming from the unilateral contacts at the feet cannot be completely alleviated. A necessary condition for static stability on a flat ground is that the ground projection of the CoM (in what follows referred to as the *gCoM*) lies within the support polygon determined as the convex hull of all contact points [36]. Henceforth, the term "base of support" (BoS), borrowed from the biomechanics literature, will be used. Note that when the gCoM is at the boundary of the BoS, even a very small disturbance wrench (e.g. stemming from an air current) may induce uncontrollable CRB roll. In order to prevent this situation, usually a safety zone is introduced within the BoS. Constraining the gCoM within the safety zone increases the robustness of the posture.

Static postural stability has to be assessed, though, not only for coplanar contacts on flat ground but also for the general noncoplanar case [52,16]. As a theoretical base, a study on "imperfect" static stability conditions within a system of multiple rigid bodies in contact under Coulomb friction can be used [55]. Accordingly, the following four contact stability conditions can be distinguished:

- *weakly stable*: a valid contact wrench exists that induces zero accelerations;
- *strongly stable*: if every valid contact wrench induces zero accelerations;
- *weakly unstable*: if not strongly stable;
- *strongly unstable*: if not weakly stable.

A valid reaction/contact wrench is a wrench $\mathcal{F}_k$ that: (1) satisfies instantaneously the equation of motion under zero initial conditions, (2) is applied along the constraint basis ${}^{k}\mathbb{B}_c$ appearing in the contact map, and (3) lies within the contact wrench cone $CWC_k$. In the case of a humanoid robot with multiple contacts, valid wrenches can be obtained from the contact state determined by the contact map/CWC pair. Since the CoM position and its ground projection play an important role for stability, the CoM contact map $\mathbb{C}_{cC}$ (cf. (2.123)) is preferably used in lieu of $\mathbb{C}_{cB}$. Static stability w.r.t. the net CRB wrench (gravity force included), $\mathcal{F}_C$, can be thus assessed via $\{\mathbb{C}_{cC}, CWC\}$. Based on this information, the reaction/contact wrenches $\overline{\mathcal{F}}^{c}$ can be determined and examined for validity. As already noted, force closure–like, strongly stable postures may not be determined for a humanoid robot in the general case [32].

### *Simple Static Stability Test Based on Wrench Distribution*

The simplest test for static stability of a given posture is to check whether the base link can be restrained to resist the CoM gravity wrench $-\mathcal{G}_C$. To this end, use can be made of the general solution to the WD problem, (3.62). The minimum-norm solution component

$$\overline{\mathcal{F}}^{ext} = \mathbb{C}_{cC}^{+}\mathcal{G}_C \tag{3.76}$$

usually yields valid contact wrenches for high-friction contacts. In the case of low-friction contacts and/or nonhorizontal contact surfaces, valid contact wrenches could be obtained by including the null-space solution component $\overline{\mathcal{F}}^{n} = \boldsymbol{N}(\mathbb{C}_{cC})\overline{\mathcal{F}}_a^c$ into the above solution. A particular solution component with appropriate weighting, e.g. as in (3.53) (cf. Fig. 3.7), could also be useful. In some cases, it might be preferable to employ a particular solution component that is *consistent with statics*. The above pseudoinverse-based solution cannot be used then, as discussed in Section 3.5.4. A suitable weighted generalized inverse is introduced in Section 5.10.4.

### *CRB-Wrench Cone and Contact-Consistent CRB Wrench*

The simple static stability test outlined above is not straightforward because of the existence of an infinite set of solutions to the WD problem. This problem can be solved by reformulating the test in terms of CRB wrenches instead of contact wrenches. A convex polyhedral wrench cone, henceforth referred to as the *CRB-wrench cone*, can be constructed from multiple point-contact PCs at the vertices of the end links, as suggested in [32]. An alternative, more straightforward approach is to obtain the CRB-wrench cone by intersecting all CWCs at the end links [14]. It is assumed that the CWCs have been calculated with the procedure described at the end of Section 3.3.2 for constructing a plane-contact CWC from point-contact convex polyhedral friction cones. The net external CRB wrench acting at the CoM is represented as in (3.56). Assume that the contact wrenches are confined within their CWCs, s.t. $\boldsymbol{U}_{CWC}\overline{\mathcal{F}}^c \preceq \boldsymbol{0}$. It follows then that the CRB wrench $\mathcal{F}_C \in \text{span}(\boldsymbol{V}_{BWC})$, where $\boldsymbol{V}_{BWC} = \mathbb{C}_{cC}\boldsymbol{U}_{CWC}^S$ denotes the span representation of the CRB-wrench cone. This implies that the net CRB wrench lies within the interior of the CRB-wrench cone, i.e. $\boldsymbol{U}_{BWC}\mathcal{F}_C \preceq \boldsymbol{0}$. The last relation provides a means to check the static stability of a posture with given contact states $\{\mathbb{C}_{cC}, CWC\}$, against the net external CRB wrench, $\mathcal{F}_C$, without having to consider the underdetermined WD problem. A CRB wrench that lies within the CRB-wrench cone, i.e.

$$\mathcal{F}_C \in \{\mathbb{C}_{cC}, BWC\}, \tag{3.77}$$

will be referred to as *contact-consistent*.

### *An Example*

As an example, consider the pushing task shown in Fig. 3.9A. Depending on the friction intensity at the feet contacts, the posture can be characterized as either strongly or weekly stable. In the former case, high friction prevents the feet from sliding. In the latter case, sliding may occur due to low friction in the horizontal direction at one of the feet or both of them. To realize the task, then, it would be important to find another posture, if it exists, that can be characterized as strongly stable, even in the presence of such a low friction. Consider the

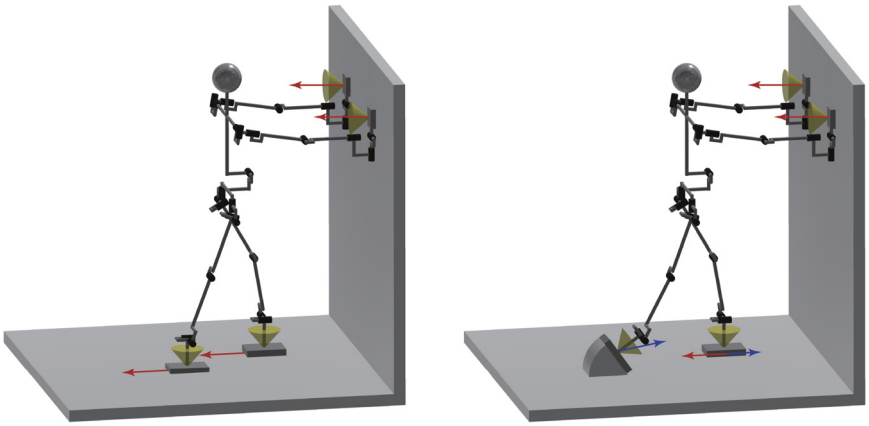

**FIGURE 3.9** Pushing task. Left (A): Reactions at the hands induce slipping forces at the feet. Right (B): Postural change with pushing leg that can generate a force opposing slip at the support leg. The cones at each end link signify surface-contact friction conditions, obtained e.g. via the CWC (cf. Section 3.3.2).

posture shown in Fig. 3.9B as a candidate. With this posture, the robot attaches its pushing leg to an inclined surface in order to generate a reaction force that opposes sliding at the support foot.

### *Contact Planning*

The last example highlights the importance of planning discrete sets of contact states [11] and respective static postures as part of the process of motion generation. The contact states may involve multiple contacts, not only at the end links but also at the intermittent links. The reason for such assumption is that the tasks of the humanoid robot should be made executable within various environments, e.g. typical for disaster scenes, involving an acyclic gait (climbing) on rough terrain [11], crawling under obstacles [71], climbing a ladder [66], and so on. The contact states are determined by a coarse model/map of the environment constructed in advance. The process is referred to as *contact planning* [23]. For each given contact state, a set of statically stable postures (or keyframes[5] [28]) is obtained. This process is referred to as the *posture generation* [13]. The posture generation is accomplished with the help of a constraint-based inverse kinematics and statics solver [6,8]. Finally, a dynamically feasible trajectory is generated to connect the keyframes by interpolation [41,28]. This approach is referred to as the "contact-before-motion" approach [29].

### *Joint Torque Limit Test*

The joint torque component $\boldsymbol{\tau}^n$ is available in the case of a kinematically redundant robot. Then, the static-equilibrium posture can be tested for compliance with the joint torque limits [53,72,20,29]. In such case, the static posture test can be based on (3.73), without any motion along the unconstrained motion directions ($\boldsymbol{\tau}^m = \mathbf{0}$), i.e.

$$\boldsymbol{\tau} = \boldsymbol{\tau}^{ext} + \boldsymbol{\tau}^{int} + \boldsymbol{\tau}^n, \tag{3.78}$$

[5] A term borrowed from the field of animation.

$$\boldsymbol{\tau}^{n} = \boldsymbol{N}(\boldsymbol{\mathcal{J}}_{cM})\,\boldsymbol{\tau}_a, \;\; |\tau_i| \leq \tau_i^{max},$$
$$\boldsymbol{\tau}^{ext} + \boldsymbol{\tau}^{int} = \boldsymbol{\mathcal{J}}_{cM}^{T}(\overline{\mathcal{F}}^{ext} + \overline{\mathcal{F}}^{n}),$$
$$\overline{\mathcal{F}}^{ext} + \overline{\mathcal{F}}^{n} = \overline{\mathcal{F}}^{c} \in CWC.$$

The Jacobian $\boldsymbol{\mathcal{J}}_{cM}$ is defined in (2.126); $\overline{\mathcal{F}}^{ext}$ is given in (3.76). The internal joint torque component $\boldsymbol{\tau}^{int} = \boldsymbol{\mathcal{J}}_{cM}^{T}\overline{\mathcal{F}}^{n}$ can be used in the contact wrench optimization; $\tau_i^{max}$ denotes the joint torque limit for joint $i$, $i \in \overline{1,n}$. Apparently, the joint torque component $\boldsymbol{\tau}^{n}(\boldsymbol{\tau}_a)$ can be used in the joint torque optimization.

### 3.7.2 Static Posture Optimization

The above formulas for static-posture stability tests provide means for optimization of: (1) the reaction forces at the contact joints (the force optimization problem [37,10]) and (2) the joint torque (redundant actuation–based optimization). The problem of force distribution optimization/control in locomotion (with a multilegged robot) and manipulation with closed kinematic chains was addressed in the pioneering work [53]. To deal with the underdetermined problem, the authors applied a linear programming with an objective function that combines energy consumption (via local power minimization) and maximum reaction (contact) force minimization.

More recent approaches to the force optimization problem have been based on a convex optimization approach [9] that involves matrix inequalities or second-order cone inequalities [10,56,12]. Standard solution algorithms for semidefinite programming problems (SDPs) or second-order cone programs (SOCPs) can then be applied. The SOCP problem can be defined as [45]

$$\min_{x} \boldsymbol{f}^{T}\boldsymbol{x}, \tag{3.79}$$

subject to

$$\|\boldsymbol{A}_i\boldsymbol{x} + \boldsymbol{b}_i\| \leq \boldsymbol{c}_i^{T}\boldsymbol{x} + d_i, \;\; i = 1, ..., N, \tag{3.80}$$

where $\boldsymbol{x} \in \Re^n$ is the optimization vector (variable), while $\boldsymbol{f} \in \Re^n$, $\boldsymbol{A}_i \in \Re^{(n_i-1)\times n}$, $\boldsymbol{b}_i \in \Re^{n_i-1}$, $\boldsymbol{c}_i \in \Re^n$, and $d_i \in \Re$ are the problem parameters (constants); $\|\circ\|$ is the standard Euclidean norm. Constraint (3.80) is called a *second-order cone constraint of dimension* $n_i$. Apparently, the friction cone constraints introduced in Section 3.3.2 can be readily represented in the above form.

In [12], for example, the so-called *support region* has been introduced to guarantee the static stability of a multipoint contact posture. The support region is defined as the 2D projection of a nonlinear convex set that is determined by the properties of each contact joint. Static posture stability is guaranteed when the CoM projection is within the support region. An iterative algorithm for convex minimization (SOCP) under inequality (friction) constraints is employed to determine the boundaries of the support region, with properly bounded error. Standard solvers, however, can be computationally demanding. This drawback has been addressed in [10], where a fast method for feasibility check was proposed based on a dual problem formulation.

It is possible to formulate the contact wrench optimization problem as a QP task (cf. (2.57)). Further details will be presented in Section 5.14.

## 3.8 POSTURE CHARACTERIZATION AND DUALITY RELATIONS

The differential-motion and kinetostatics relations, treated in Chapter 2 and the present one, respectively, can be characterized as dual relations. These relations were derived in coordinate form, referring either to the base-link frame $\{B\}$ or the CRB one, $\{C\}$. Five transforms were involved in each case. In the notation w.r.t. $\{B\}$, for example, these are the three Jacobian matrices $\boldsymbol{\mathcal{J}}_{cB}(\boldsymbol{q})$, $\boldsymbol{\mathcal{J}}_{mB}(\boldsymbol{q})$, $\boldsymbol{J}_B(\boldsymbol{q})$ and the two contact maps $\mathbb{C}_{cB}(\boldsymbol{q})$ and $\mathbb{C}_{mB}(\boldsymbol{q})$. The three Jacobians are characterized by a complementarity condition: any two will specify the third one uniquely. Contact maps $\mathbb{C}_{cB}(\boldsymbol{q})$ and $\mathbb{C}_{mB}(\boldsymbol{q})$ are also complementary. In the following analysis, $\boldsymbol{\mathcal{J}}_{cB}(\boldsymbol{q})$, $\boldsymbol{J}_B(\boldsymbol{q})$, and $\mathbb{C}_{cB}(\boldsymbol{q})$ will be employed as *fundamental* transforms that provide complete insight into the differential kinematics and kinetostatics relations. They also play an important role in dynamic relations.

The above transforms are functions of the generalized coordinates that determine the robot's posture in a unique way. Typical postures are listed in Table 3.1. A *regular posture* is characterized by the base link being mobile in any direction. This implies that the row space of contact map $\mathbb{C}_{cB}$ should be a subspace of the range (column) space of the constraint Jacobian $\boldsymbol{\mathcal{J}}_{cB}$. At a multicontact posture, the base-link motion can be generated only with constraint-consistent joint velocities. When the regular-posture condition is not satisfied, the posture is characterized as *singular*. For example, when pushing a heavy object, (near) singular arm/leg configurations are used. Then, one or more of the limb Jacobians, $\boldsymbol{J}_B(\boldsymbol{q}_{e_j})$, (and hence, the constraint Jacobian $\boldsymbol{\mathcal{J}}_{cB}$) will be rank-deficient. The mobility of the base link will be then constrained: a solution to the inverse kinematics problem might not exist when the base-link velocity is assigned in an arbitrary way. Further on, at a singular posture, the force impressed on the base link from the respective end links becomes a *structural force*, according to the structural-force posture condition shown in Table 3.1.[6] For instance, the quiet-stance upright posture with straightened legs induces a structural-force pattern w.r.t. the force of gravity.

Next, an *internal-wrench* posture is a multicontact posture, s.t. the contact wrenches sum up to yield a nonzero net wrench on the base link (CRB wrench). In this case, the contact wrenches can be used to ensure that the friction cone conditions are met. At an internal joint torque posture, on the other hand, motor-load redistribution can be achieved, e.g. to avoid the joint torque limits and/or to minimize the joint torques (cf. (3.73)). Note that sometimes the term "overactuation" appears in texts referring to redundant actuation (a local, posture-dependent characteristic). This may lead to confusion, though, since a humanoid robot is characterized as an underactuated system (a global, posture-independent characteristic).

The next three postures in Table 3.1 refer to the types of motion constraints imposed on the base via the contact joints. When the robot is in a static single-stance posture with planar contact, the foot can be assumed to be fixed to the ground as long as the gCoM is within

[6] This term is borrowed from grasp analysis [49].

**TABLE 3.1** Types of humanoid robot postures

| Posture | Condition | Characterization |
|---|---|---|
| regular | $\mathcal{R}(\mathbb{C}_{cB}^T) \subset \mathcal{R}(\boldsymbol{\mathcal{J}}_{cB})$ | base motion possible in any direction |
| singular | $\mathcal{R}(\mathbb{C}_{cB}^T) \not\subset \mathcal{R}(\boldsymbol{\mathcal{J}}_{cB})$ | impossible base motion in some directions |
| structural force | $\mathbb{C}_{cB}^{+}\mathcal{F}_B \in \mathcal{N}^*(\boldsymbol{\mathcal{J}}_{cB}{}^T)$ | external forces are resisted without motor load |
| internal wrench | $\overline{\mathcal{F}}^n \notin \mathcal{N}^*(\mathbb{C}_{cB}) \cap CWC$ | a nonzero CRB wrench is generated |
| internal joint torque | $\boldsymbol{\tau}^n \in \mathcal{N}^*(\boldsymbol{J}_B)$ | does not alter the end-link wrench |
| fully constrained (unilaterally) | $c = 6$ (single stance) | any joint velocity admissible |
| overconstrained (unilaterally) | $c > 6$ (double stance) | only constraint-consistent joint vel. admissible |
| underconstrained | $c < 6,\ \mathcal{V}_B \in \mathcal{N}(\mathbb{C}_{cB}^T)$ | base motion resulting from lack of constraints |
| stationary base | $\dot{\boldsymbol{\theta}} \in \mathcal{N}(\boldsymbol{\mathcal{J}}_{cB})$ | end-link and internal-link motion |
| stationary base and end links | $\dot{\boldsymbol{\theta}} \in \mathcal{N}(\boldsymbol{J}_B)$ | internal-link motion only |
| stationary end links | $\dot{\boldsymbol{\theta}} \in \mathcal{N}(\boldsymbol{J}_B) \cap \mathcal{R}(\boldsymbol{\mathcal{J}}_{cB}^T)$ | internal-link motion with mobile base |

the BoS. This posture is characterized as a *(unilaterally) fully constrained* posture: there are no closed loops and, therefore, any joint velocity is admissible. When in double stance, on the other hand, the posture is characterized as *unilaterally overconstrained*: there is a closed loop and, therefore, only constraint-consistent joint velocities are admissible. Furthermore, for a posture, s.t. the gCoM is at the BoS boundary, an arbitrary small disturbance may induce a change in the contact joint type (e.g. from planar to line or point contact). The posture then becomes *underconstrained*: there is at least one base mobility direction that cannot be constrained via the contacts. Such a posture may eventually result in a fall. Another example of an underconstrained posture is when the robot is in mid-air, i.e. while running or jumping. Then, all six mobility directions of the base link are unconstrained. Note that the term "underconstrained" should not be confused with "underactuated." The former, being posture-dependent, provides a local characterization while the latter refers to a global feature: there are no actuators attached to the base.

Next, a *stationary-base* posture is characterized by motion in the links whereby the base remains stationary. When the motion is obtained with joint velocities from the null space of the joint-space constraint Jacobian, the end links will move. The associated motion patterns are "motion with stationary base" (e.g. limb self-motion) and "end-link motion with stationary base." Further restricting the joint velocities to the null space of the complete Jacobian immobilizes the end links; the only associated motion pattern is "limb self-motion." At such a posture, an internal-link motion is available for obstacle and/or singularity avoidance and other secondary subtasks in the *motion* domain.

Fig. 3.10 displays a graphic representation of the conditions along with representative postures from the subspaces of the three fundamental transforms. The transforms decompose the joint, the end-link, and the base-link spaces as follows. The joint space is decomposed in two ways, by $\boldsymbol{\mathcal{J}}_{cB}$ and $\boldsymbol{J}_B$. The end-link space is also decomposed in two ways, by $\boldsymbol{\mathcal{J}}_{cB}$ and $\mathbb{C}_{cB}$. The base-link space is decomposed by $\mathbb{C}_{cB}$ only. The right angles signify the orthogonality relations pertinent to the fundamental subspaces of the transforms.

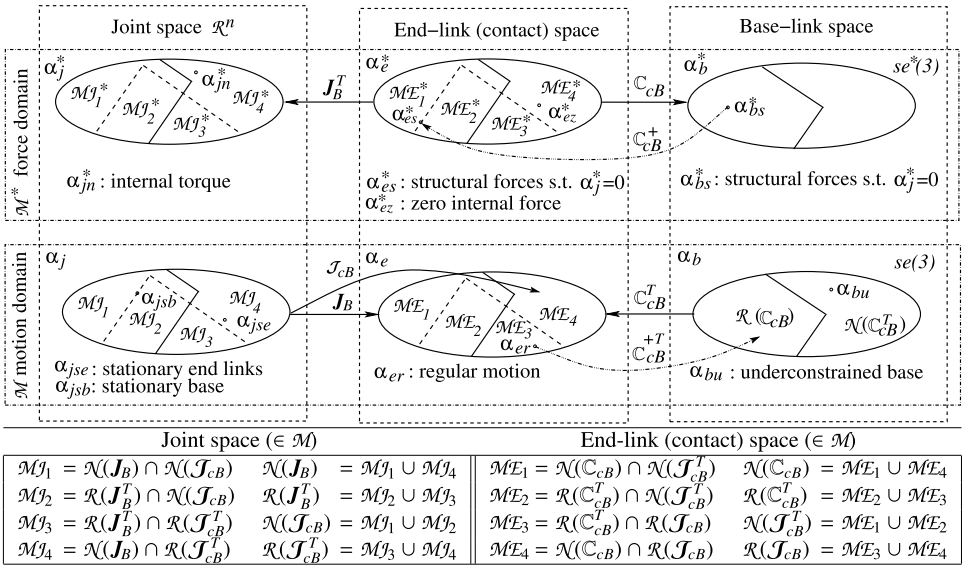


**FIGURE 3.10** Joint space, end-link (contact) space, and base-link space with their dual motion/force subspaces. Right angles signify orthogonality decompositions stemming from the three fundamental transforms, $\boldsymbol{\mathcal{J}}_{cB}$, $\boldsymbol{J}_B$, and $\mathbb{C}_{cB}$. The table explains the meaning of the subspace notation in the motion subdomain. The respective meaning in the force subdomain is analogous. The $\alpha$s denote motion elements (velocities), the $\alpha^*$s are their duals (forces). Representative postures are specified according to the relations in Table 3.1.

## References


[1] Y. Abe, M. Da Silva, J. Popović, Multiobjective control with frictional contacts, in: ACM SIGGRAPH/Eurographics Symposium on Computer Animation, 2007, pp. 249–258.

[2] M. Anitescu, F.A. Potra, Formulating dynamic multi-rigid-body contact problems with friction as solvable linear complementarity problems, Nonlinear Dynamics 14 (1997) 231–247.

[3] D.J. Balkcom, J. Trinkle, Computing wrench cones for planar rigid body contact tasks, The International Journal of Robotics Research 21 (2002) 1053–1066.

[4] R. Ball, The Theory of Screws: A Study in the Dynamics of a Rigid Body, Hodges, Foster, and Company, 1876.

[5] D. Baraff, Fast contact force computation for nonpenetrating rigid bodies, in: 21st Annual Conference on Computer Graphics and Interactive Techniques – SIGGRAPH '94, ACM Press, New York, New York, USA, 1994, pp. 23–34.

[6] K. Bouyarmane, A. Kheddar, Static multi-contact inverse problem for multiple humanoid robots and manipulated objects, in: IEEE-RAS International Conference on Humanoid Robots, Nashville, TN, USA, 2010, pp. 8–13.

[7] K. Bouyarmane, A. Kheddar, Using a multi-objective controller to synthesize simulated humanoid robot motion with changing contact configurations, in: IEEE/RSJ International Conference on Intelligent Robots and Systems, 2011, pp. 4414–4419.

[8] K. Bouyarmane, A. Kheddar, Humanoid robot locomotion and manipulation step planning, Advanced Robotics 26 (2012) 1099–1126.

[9] S.P. Boyd, L. Vandenberghe, Convex Optimization, Cambridge University Press, 2004.

[10] S.P. Boyd, B. Wegbreit, Fast computation of optimal contact forces, IEEE Transactions on Robotics 23 (2007) 1117–1132.

[11] T. Bretl, Motion planning of multi-limbed robots subject to equilibrium constraints: the free-climbing robot problem, The International Journal of Robotics Research 25 (2006) 317–342.

[12] T. Bretl, S. Lall, Testing static equilibrium for legged robots, IEEE Transactions on Robotics 24 (2008) 794–807.

[13] S. Brossette, A. Escande, G. Duchemin, B. Chrétien, A. Kheddar, Humanoid posture generation on non-Euclidean manifolds, in: IEEE-RAS International Conference on Humanoid Robots, 2015, pp. 352–358.
[14] S. Caron, Q. Cuong Pham, Y. Nakamura, Leveraging cone double description for multi-contact stability of humanoids with applications to statics and dynamics, in: Robotics: Science and Systems XI, Rome, Italy, 2015, pp. 28–36.
[15] S. Caron, Q.-C. Pham, Y. Nakamura, Stability of surface contacts for humanoid robots: closed-form formulae of the contact wrench cone for rectangular support areas, in: IEEE International Conference on Robotics and Automation, Seattle, Washington, USA, 2015, pp. 5107–5112.
[16] S. Caron, Q.-C. Pham, Y. Nakamura, ZMP support areas for multicontact mobility under frictional constraints, IEEE Transactions on Robotics 33 (2017) 67–80.
[17] J.-R. Chardonnet, S. Miossec, A. Kheddar, H. Arisumi, H. Hirukawa, F. Pierrot, K. Yokoi, Dynamic simulator for humanoids using constraint-based method with static friction, in: IEEE International Conference on Robotics and Biomimetics, 2006, pp. 1366–1371.
[18] C. Collette, A. Micaelli, C. Andriot, P. Lemerle, Dynamic balance control of humanoids for multiple grasps and non coplanar frictional contacts, in: IEEE-RAS International Conference on Humanoid Robots, 2007, pp. 81–88.
[19] J.K. Davidson, K.H. Hunt, Robots and Screw Theory: Applications of Kinematics and Statics to Robotics, Oxford University Press, 2004.
[20] P.G. De Santos, J. Estremera, E. Garcia, M. Armada, Including joint torques and power consumption in the stability margin of walking robots, Autonomous Robots 18 (2005) 43–57.
[21] K.L. Doty, C. Melchiorri, C. Bonivento, A theory of generalized inverses applied to robotics, The International Journal of Robotics Research 12 (1993) 1–19.
[22] J. Duffy, The fallacy of modern hybrid control theory that is based on "orthogonal complements" of twist and wrench spaces, Journal of Robotic Systems 7 (1990) 139–144.
[23] A. Escande, A. Kheddar, S. Miossec, Planning contact points for humanoid robots, Robotics and Autonomous Systems 61 (2013) 428–442.
[24] R. Featherstone, Rigid Body Dynamics Algorithms, Springer Science+Business Media, LLC, Boston, MA, 2008.
[25] Fujitsu, Miniature Humanoid Robot HOAP-2 Manual, 1st edition, Fujitsu Automation Co., Ltd, 2004 (in Japanese).
[26] cdd and cddplus homepage, https://www.inf.ethz.ch/personal/fukudak/cdd_home/ [online].
[27] K. Harada, M. Kaneko, Analysis of internal force in whole body manipulation by a human type robotic mechanisms, Journal of the Robotics Society of Japan 21 (2003) 647–655 (in Japanese).
[28] K. Hauser, Fast interpolation and time-optimization with contact, The International Journal of Robotics Research 33 (2014) 1231–1250.
[29] K. Hauser, T. Bretl, J.C. Latombe, Non-gaited humanoid locomotion planning, in: IEEE-RAS International Conference on Humanoid Robots, 2005, pp. 7–12.
[30] K. Hauser, T. Bretl, J.-C. Latombe, K. Harada, B. Wilcox, Motion planning for legged robots on varied terrain, The International Journal of Robotics Research 27 (2008) 1325–1349.
[31] S. Hirai, Analysis and Planning of Manipulation Using the Theory of Polyhedral Convex Cones, Ph.D. thesis, Kyoto University, 1991.
[32] H. Hirukawa, S. Hattori, K. Harada, S. Kajita, K. Kaneko, F. Kanehiro, K. Fujiwara, M. Morisawa, A universal stability criterion of the foot contact of legged robots – adios ZMP, in: IEEE International Conference on Robotics and Automation, 2006, pp. 1976–1983.
[33] M. Hosokawa, D. Nenchev, Sliding control with a double-stance posture on V-shaped support, Robotic Life Support Laboratory, Tokyo City University, 2017 (Video clip), https://doi.org/10.1016/B978-0-12-804560-2.00010-9.
[34] S.-H. Hyon, J. Hale, G. Cheng, Full-body compliant human-humanoid interaction: balancing in the presence of unknown external forces, IEEE Transactions on Robotics 23 (2007) 884–898.
[35] Y. Jun, A. Alspach, P. Oh, Controlling and maximizing humanoid robot pushing force through posture, in: 9th International Conference on Ubiquitous Robots and Ambient Intelligence, URAI, 2012, pp. 158–162.
[36] S. Kajita, H. Hirukawa, K. Harada, K. Yokoi, Introduction to Humanoid Robotics, Springer Verlag, Berlin, Heidelberg, 2014.
[37] J. Kerr, B. Roth, Analysis of multifingered hands, The International Journal of Robotics Research 4 (1986) 3–17.
[38] O. Khatib, A unified approach for motion and force control of robot manipulators: the operational space formulation, IEEE Journal on Robotics and Automation 3 (1987) 43–53.

[39] E. Kokkevis, Practical physics for articulated characters, in: Game Developers Conference, 2004, 2004, pp. 1–16.
[40] T. Koolen, S. Bertrand, G. Thomas, T. de Boer, T. Wu, J. Smith, J. Englsberger, J. Pratt, Design of a momentum-based control framework and application to the humanoid robot Atlas, International Journal of Humanoid Robotics 13 (2016) 1650007.
[41] J.J. Kuffner, S. Kagami, K. Nishiwaki, M. Inaba, H. Inoue, Dynamically-stable motion planning for humanoid robots, Autonomous Robots 12 (2002) 105–118.
[42] S. Kuindersma, R. Deits, M. Fallon, A. Valenzuela, H. Dai, F. Permenter, T. Koolen, P. Marion, R. Tedrake, Optimization-based locomotion planning, estimation, and control design for the atlas humanoid robot, Autonomous Robots 40 (2016) 429–455.
[43] V. Kumar, K. Waldron, Force distribution in closed kinematic chains, IEEE Journal on Robotics and Automation 4 (1988) 657–664.
[44] S.-H.H. Lee, A. Goswami, A momentum-based balance controller for humanoid robots on non-level and non-stationary ground, Autonomous Robots 33 (2012) 399–414.
[45] M.S. Lobo, L. Vandenberghe, S. Boyd, H. Lebret, Applications of second-order cone programming, Linear Algebra and Its Applications 284 (1998) 193–228.
[46] N. Mansard, O. Khatib, Continuous control law from unilateral constraints, in: IEEE International Conference on Robotics and Automation, 2008, pp. 3359–3364.
[47] D. Mansour, A. Micaelli, P. Lemerle, A computational approach for push recovery in case of multiple noncoplanar contacts, in: IEEE/RSJ International Conference on Intelligent Robots and Systems, IEEE, San Francisco, CA, USA, 2011, pp. 3213–3220.
[48] M. Murooka, S. Nozawa, Y. Kakiuchi, K. Okada, M. Inaba, Whole-body pushing manipulation with contact posture planning of large and heavy object for humanoid robot, in: IEEE International Conference on Robotics and Automation, 2015, pp. 5682–5689.
[49] R.M. Murray, Z. Li, S.S. Sastry, A Mathematical Introduction to Robotic Manipulation, CRC Press, 1994.
[50] Y. Nakamura, Minimizing object strain energy for coordination of multiple robotic mechanisms, in: American Control Conference, Atlanta, GA, USA, 1988, pp. 499–509.
[51] S. Nakaoka, S. Hattori, F. Kanehiro, S. Kajita, H. Hirukawa, Constraint-based dynamics simulator for humanoid robots with shock absorbing mechanisms, in: IEEE/RSJ International Conference on Intelligent Robots and Systems, San Diego, CA, USA, 2007, pp. 3641–3647.
[52] Y. Or, E. Rimon, Computation and graphical characterization of robust multiple-contact postures in two-dimensional gravitational environments, The International Journal of Robotics Research 25 (2006) 1071–1086.
[53] D.E. Orin, S.Y. Oh, Control of force distribution in robotic mechanisms containing closed kinematic chains, Journal of Dynamic Systems, Measurement, and Control 103 (1981) 134–141.
[54] C. Ott, M.A. Roa, G. Hirzinger, Posture and balance control for biped robots based on contact force optimization, in: IEEE-RAS International Conference on Humanoid Robots, Bled, Slovenia, 2011, pp. 26–33.
[55] J.-S. Pang, J. Trinkle, Stability characterizations of rigid body contact problems with Coulomb friction, ZAMM – Zeitschrift für Angewandte Mathematik und Mechanik (Journal of Applied Mathematics and Mechanics) 80 (2000) 643–663.
[56] I.-W. Park, J.-Y. Kim, J. Lee, J.-H. Oh, Mechanical design of the humanoid robot platform HUBO, Advanced Robotics 21 (2007) 1305–1322.
[57] J. Park, Control Strategies for Robots in Contact, Ph.D. thesis, Stanford University, USA, 2006.
[58] J.K. Salisbury, J.J. Craig, Articulated hands: force control and kinematic issues, The International Journal of Robotics Research 1 (1982) 4–17.
[59] L. Sentis, O. Khatib, Compliant control of multicontact and center-of-mass behaviors in humanoid robots, IEEE Transactions on Robotics 26 (2010) 483–501.
[60] B. Siciliano, O. Khatib (Eds.), Handbook of Robotics, Springer Verlag, Berlin, Heidelberg, 2008.
[61] W. Son, K. Kim, N.M. Amato, J.C. Trinkle, A generalized framework for interactive dynamic simulation for multirigid bodies, IEEE Transactions on Systems, Man and Cybernetics. Part B. Cybernetics 34 (2004) 912–924.
[62] D.E. Stewart, J.C. Trinkle, An implicit time-stepping scheme for rigid body dynamics with inelastic collisions and coulomb friction, International Journal for Numerical Methods in Engineering 39 (1996) 2673–2691.
[63] J.C. Trinkle, J.-S. Pang, S. Sudarsky, G. Lo, On dynamic multi-rigid-body contact problems with Coulomb friction, ZAMM – Zeitschrift für Angewandte Mathematik und Mechanik (Journal of Applied Mathematics and Mechanics) 77 (1997) 267–279.

[64] J.C. Trinkle, J.A. Tzitzouris, J.S. Pang, Dynamic multi-rigid-body systems with concurrent distributed contacts, Philosophical Transactions of the Royal Society of London A: Mathematical, Physical and Engineering Sciences 359 (2001) 2575–2593.
[65] M. Uchiyama, P. Dauchez, Symmetric kinematic formulation and non-master/slave coordinated control of two-arm robots, Advanced Robotics 7 (1992) 361–383.
[66] J. Vaillant, A. Kheddar, H. Audren, F. Keith, S. Brossette, A. Escande, K. Bouyarmane, K. Kaneko, M. Morisawa, P. Gergondet, E. Yoshida, S. Kajita, F. Kanehiro, Multi-contact vertical ladder climbing with an HRP-2 humanoid, Autonomous Robots 40 (2016) 561–580.
[67] M.W. Walker, D.E. Orin, Efficient dynamic computer simulation of robotic mechanisms, Journal of Dynamic Systems, Measurement, and Control 104 (1982) 205.
[68] P.M. Wensing, G. Bin Hammam, B. Dariush, D.E. Orin, Optimizing foot centers of pressure through force distribution in a humanoid robot, International Journal of Humanoid Robotics 10 (2013) 1350027.
[69] D. Williams, O. Khatib, The virtual linkage: a model for internal forces in multi-grasp manipulation, in: IEEE International Conference on Robotics and Automation, Atlanta, GA, USA, 1993, pp. 1025–1030.
[70] K. Yamane, Y. Nakamura, A numerically robust LCP solver for simulating articulated rigid bodies in contact, in: Robotics: Science and Systems IV, MIT Press, Zurich, Switzerland, 2008, pp. 89–104.
[71] K. Yokoi, E. Yoshida, H. Sanada, Unified motion planning of passing under obstacles with humanoid robots, in: IEEE International Conference on Robotics and Automation, 2009, pp. 1185–1190.
[72] Y. Yokokohji, S. Nomoto, T. Yoshikawa, Static evaluation of humanoid robot postures constrained to the surrounding environment through their limbs, in: IEEE International Conference on Robotics and Automation, 2002, pp. 1856–1863.
[73] Yu Zheng, K. Yamane, Y. Zheng, K. Yamane, Human motion tracking control with strict contact force constraints for floating-base humanoid robots, in: IEEE-RAS International Conference on Humanoid Robots, Atlanta, GA, USA, 2013, pp. 34–41.
[74] Y. Zheng, C.-M. Chew, Fast equilibrium test and force distribution for multicontact robotic systems, Journal of Mechanisms and Robotics 2 (2010) 021001.
[75] Y. Zheng, J. Luh, Joint torques for control of two coordinated moving robots, in: IEEE International Conference on Robotics and Automation, 1986, pp. 1375–1380.
[76] D. Zlatanov, D.N. Nenchev, On the use of metric-dependent methods in robotics, in: ASME Proceedings, 5th International Conference on Multibody Systems, Nonlinear Dynamics and Control, vol. 6, ASME, 2005, pp. 703–710.